

27 **1. Abstract**

28 The assessment of the seismic vulnerability of unreinforced masonry
29 (URM) structures based on numerical modeling constitutes a difficult task due to
30 their complex behavior, especially in the nonlinear dynamic field, and the lack of
31 suitable, low-demanding, computational tools. In the last decades, practical
32 statistical tools for the derivation of fragility curves has been successfully proposed
33 mainly with reference to framed structures. This approach has been adopted also
34 for the seismic vulnerability assessment of masonry buildings focusing on the in-
35 plane collapse mechanisms by means of equivalent frame models. Nevertheless,
36 the lack of computationally effective tools which involve the interaction between
37 in-plane and out-of-plane mechanisms makes the definition of fragility curve an
38 arduous task when it comes to existing masonry structures without box behavior.

39 In this paper, a practical and thorough methodology for the assessment of
40 the seismic vulnerability of URM buildings by means of analytical fragility curves
41 is presented. This methodology presents some innovative features such as the
42 definition of the limit states (LSs) and their corresponding capacity based on
43 multi-directional pushover analyses, as well as the application of nonlinear
44 dynamic analyses, performed using a discrete macro-element modelling approach
45 capable of simulating the main in-plane and out-of-plane responses of URM
46 structures with a reduced computational burden. The present investigation
47 focuses on the application of this methodology for assessing the seismic
48 vulnerability of a brick masonry structure characterized by a strong out-of-plane
49 failure mechanism. After a fitting process, the fragility curves were compared to
50 the ones obtained using expert-based approaches.

51

52 *Keywords:* Brick masonry structure, Multi-directional pushover analysis,
53 Nonlinear dynamic analysis, Displacement capacity, Analytical fragility curves,
54 HiStrA software.

55 1. Introduction

56 Masonry buildings constitute the most scattered low-rise structural
57 typology in the world, mainly because of its economic affordability and
58 constructive ease. In addition to residential buildings, the vast majority of heritage
59 constructions, usually made of brick, stone or adobe, also belong to this structural
60 typology. These structures are often located in areas with high seismic activity,
61 and most of them were built without following specific seismic design standards.
62 It is well-known that, besides being an important cause of human losses,
63 earthquakes constitute a major threat involving the stability of this typology of
64 structures. Therefore, the seismic vulnerability assessment of this structural
65 typology is a relevant topic within the different fields concerning decision making,
66 risk prediction and management of seismic hazard. Nevertheless, masonry
67 structures present a response difficult to predict due to the high uncertainty
68 associated with variables such as their mechanical, geometrical or structural
69 parameters, or load conditions to which they are subjected to. Considering the high
70 uncertainty of this type of buildings, deterministic approaches are less suitable for
71 assessing the seismic vulnerability of URM structures. In this sense, stochastic-
72 probabilistic methodologies are desirable to better understand the seismic
73 vulnerability assessment of this type of structures [1].

74 Seismic vulnerability assessment is often performed using practical
75 statistical tools such as fragility functions which allow the estimation of the
76 probability of reaching or exceeding a limit state (LS) due to a given Intensity
77 Measure (IM) [2]. Fragility functions can be defined following different
78 approaches, namely expert-based, analytical, empirical and hybrid
79 formulations [3]. The definition of fragility functions by means of expert-based
80 formulations involves a substantial and detailed assessment of an estimate of
81 damage level provided by a team of experts [4]. Nevertheless, due to the diverse
82 individual experiences of the experts, damage estimates with a high level of
83 consensus may not be reached, making this type of formulation somehow limited.
84 On the other hand, empirical-based fragility functions involve a statistical
85 elaboration of data obtained from post-earthquake surveys. This type of
86 formulation is based on a more realistic source of information (such as structural

87 typologies, soil effects and site characteristics) allowing a more accurate
88 assessment of the seismic vulnerability. Fragility functions derived from
89 analytical formulations involve the development of structural models and the
90 subsequent performing of numerical simulations. Even though this type of
91 fragility functions may increase the reliability of the seismic vulnerability
92 assessment by reducing the bias associated with expert-based formulations, its
93 derivation still presents some important limitations. Sophisticated numerical
94 tools require a significantly large computational burden and the extensive
95 knowledge of input parameters. Furthermore, most simplified models currently
96 used for the numerical simulations are not capable of providing a realistic
97 prediction of the earthquake structural response since they neglect the interaction
98 between in-plane and out-of-plane mechanisms.

99 Another important aspect that plays a fundamental role in the assessment
100 of seismic vulnerability, based on nonlinear analyses, corresponds to the definition
101 of appropriate IMs and LSs. Macroscale intensity measures as the Peak Ground
102 Acceleration (PGA) constitute parameters commonly used for the derivation of
103 fragility functions due to the simple physical meaning they provide [5]. Other
104 parameters such as the peak ground velocity, the spectral acceleration or spectral
105 displacement, the Arias and Housner intensities have been considered as IMs for
106 seismic vulnerability assessment [6]. LSs are related to the response of a building,
107 and they are commonly based on its structural performance. This performance is
108 often related to interstory drifts formulations as specified in different codes or
109 standards [7-11] or proposed by different authors [12-15]. The most common
110 formulation for assessing the seismic vulnerability of masonry structures is based
111 on the interstory drift capacity. As reported in the EC8-Part3 [9], the definition of
112 this displacement-based formulation is associated with the type of mechanism
113 governing the collapse of the structure. For instance, a lateral drift of 0.4% is
114 proposed for a Significant Damage LS when the structure experiences a shear
115 failure, and 0.8% (H_0/L) when the collapse is ruled by a flexural mechanism, being
116 H_0 and L the distance between the contra-flexure point and the point in which the
117 flexural capacity is attained, and the in-plane length of the wall, respectively. It is
118 worth to note that similar failure mechanism-based procedures have been adopted

119 by additional standards such as Italian Code [11], FEMA 273 [7] and FEMA 306
120 [8]. A summary of the different interstory drift-based procedures and a detailed
121 comparison can be found in the work presented by Petry and Beyer [16]. On the
122 other hand, a multiscale approach was proposed in [17, 18] for the definition of
123 LSs. This approach involves the structure performance assessment at three
124 different levels: i) local, ii) global, and iii) macro-element. The application of this
125 approach is mainly suitable for multistory masonry buildings in which the global
126 behavior is most influenced by the in-plane response of masonry walls. The
127 assessment of buildings characterized by flexible diaphragms or by the absence of
128 diaphragms requires additional criteria. In this regard, the authors have proposed
129 the application of macro block models in order to assess the out-of-plane
130 mechanisms of this type of buildings and its integration with the multiscale
131 approach.

132 Very few studies are devoted to the assessment of the seismic vulnerability
133 of unreinforced masonry buildings based on fragility functions [19]. Rota, et al. [5]
134 investigated the seismic vulnerability of some typical Italian masonry structures
135 using empirical fragility functions. The derivation of such functions was based on
136 post-earthquake damage data relative to 91,934 buildings, classified into twenty-
137 three structural typologies, and the definition of five LSs in accordance with the
138 European Macroseismic Scale [20]. The seismic vulnerability assessment required
139 the formulation of Damage Probability Matrices for each structural typology and
140 PGA interval. A similar investigation regarding Iranian buildings was carried out
141 by Omidvar, et al. [21] in 2012.

142 The seismic vulnerability of masonry structures has also been investigated
143 by means of analytical formulations and the use of simplified computational tools.
144 For instance, Park, et al. [22] investigated the seismic vulnerability of low-rise
145 URM buildings located in the central and southern regions of the US using
146 simplified numerical models. In this sense, the walls loaded in the in-plane
147 direction were modeled as an arrangement of nonlinear links in series, whereas
148 the walls loaded in the out-of-plane direction and horizontal diaphragms were
149 simulated as single nonlinear links. Four LSs together with their corresponding

150 interstory drift capacities were established in accordance with specifications
151 provided by HAZUS [23].

152 Pasticier, et al. [24] investigated the seismic vulnerability of a typical two-
153 story stone masonry building using an equivalent frame modeling approach,
154 performed with the software SAP2000 [25], consistent with the three LSs defined
155 in the EC8-Part3 [9]. The global behavior of the building was firstly investigated
156 through static pushover analyses. Subsequently, a simplified model of the
157 building's façade was subjected to Incremental Dynamic Analysis (IDA) based on
158 fourteen earthquake ground motion records with different scaling factors. In such
159 investigation, the uncertainty was focused on the PGA, which was also considered
160 as IM.

161 Asteris [14] defined specific damage states for the evaluation of the seismic
162 vulnerability of masonry structures. These states were used for the seismic
163 assessment of a Greek historical monastery [26]. In such investigation, fragility
164 curves were derived by means of FE numerical simulations. The seismic
165 vulnerability also involved the use of different restoration mortars in order to
166 determine the best alternative for strengthening purposes. The mortars were
167 obtained by means of an inverse engineering procedure aiming at assuring their
168 compatibility with the original constituent material [27]. Asteris, et al. [28] also
169 investigated the seismic vulnerability of historical masonry structures located in
170 Portugal, Cyprus and Greece. Numerical models of these masonry structures,
171 based on the FE method, were used for the generation of fragility curves. In a more
172 recent investigation, Asteris, et al. [1] presented a methodology for seismic
173 vulnerability assessment which involves activities such as geometrical
174 reconstruction, mechanical characterization, numerical modeling, definition of
175 seismic actions and failure criteria, application of strengthening techniques, and
176 derivation of fragility curves. The latter investigation also considered that the
177 limit states were based on a damage-based approach. The methodology was
178 applied to a set of masonry walls considering uncertainty related to tensile
179 strength, percentage of openings, and peak ground acceleration.

180 The seismic vulnerability of an Italian typological three-story masonry
181 building was assessed by Rota, et al. [19]. An equivalent frame computational

182 model, implemented in the software TreMuri [29], was subjected to static and
183 dynamic nonlinear analyses. The application of pushover analyses was based on
184 an incremental lateral force proportional to the first vibration mode, whereas the
185 time history analyses involved real ground motion records properly scaled to
186 match the response spectrum.

187 Erberik [30] assessed the seismic vulnerability of Turkish masonry
188 buildings through the application of static and dynamic nonlinear analyses using
189 the software SAM [31]. The buildings were classified into different groups
190 considering criteria such as the number of stories, material, length of walls and
191 openings and regularity in plan. Two shear capacity-based LSs and PGA as IM,
192 which ranged between 0.01 g and 0.80 g, were established for the assessment of
193 the seismic vulnerability of such structures. Additional investigation associated
194 with masonry structures can be found in [32-34].

195 Most of the investigations conducted so far are based on simplified
196 numerical models which do not allow to consider the interaction between in-plane
197 and out-of-plane mechanisms. In addition, they mainly focused on the seismic
198 response of URM structure due to the application of nonlinear static analysis,
199 which neglects the degradation of stiffness and strength due to the unloading and
200 reloading cycles. In this sense, the assessment of the seismic vulnerability of URM
201 structures requires thorough methodologies based on the use of numerical
202 strategies able to provide a more realistic earthquake response still maintaining
203 a low computational burden. This paper aims at proposing a methodology for the
204 seismic vulnerability assessment of an URM structure using a simplified
205 computational tool capable of simulating the in-plane and out-of-plane
206 mechanisms. The computational tool, named Discrete Macro-Element
207 Modeling (DMEM) approach, is also characterized by a reduced number of degrees
208 of freedom (DOFs) which allows the application of nonlinear dynamic analysis
209 with a low computational demand. In addition, a multidirectional pushover
210 analysis technique is used for the definition of the displacement capacity of the
211 URM structure. Based on the results of this investigation, it was possible to
212 demonstrate the applicability of this methodology for the assessment of the
213 seismic vulnerability of URM structures.

214 **2. The Discrete Macro-Element Modeling (DMEM)** 215 **approach**

216 An alternative modeling approach for assessing the in-plane response of
217 masonry structures was initially introduced by Calio, et al. [35] in which masonry
218 structures were represented by means of two-dimensional panels. Each panel can
219 be represented according to a mechanical scheme composed by a rigid hinged
220 quadrilateral and two diagonal nonlinear links. As depicted in Figure 1a, the
221 connection between two adjacent panels is ruled by a zero-thickness interface
222 discretized with a number of nonlinear links placed in the direction orthogonal to
223 its length and a single nonlinear link placed along its length.

224 This simplified modeling approach is capable of simulating the main in-
225 plane failure mechanisms of masonry structures which are governed by a different
226 set of nonlinear links. The flexural mechanism, associated with the crushing of
227 masonry in the compressive area and the rupture in the tensile area, is governed
228 by the nonlinear links orthogonally distributed along the length of the interface
229 element. The in-plane shear-sliding mechanism or slipping of masonry in the
230 direction parallel to the mortar joints, which occurs for low values of cohesion or
231 friction force, is simulated by means of the single sliding nonlinear link in the
232 interface element. Finally, the in-plane shear-diagonal mechanism, related to the
233 formation of diagonal cracking, as a consequence of low values of tensile strength,
234 is ruled by the couple of diagonal nonlinear links at the panel. The kinematics of
235 each panel is described by four Lagrangian parameters associated with the rigid
236 body motion and the shear deformability of a masonry panel.

237 The plane mechanical scheme can be efficiently adopted for describing the
238 global response of masonry buildings governed by the in-plane behavior of
239 masonry walls assuming that the out-of-plane mechanics are prevented. In order
240 to overcome this significant restriction, an upgrade of the plane element was
241 carried out by Pantò, et al. [36]. The extension of the element to spatial behavior
242 has been obtained by introducing two-dimensional interface element
243 characterized by new sets of nonlinear links allowing the simulation of out-of-
244 plane mechanisms. The two-dimensional interface element is now discretized into
245 a matrix of transversal nonlinear links which aim at governing the bi-flexural

246 mechanism of this type of structures. The out-of-plane sliding and the torsional
 247 responses of URM structures are simulated by two additional links which are
 248 placed along the thickness of the interface element. As illustrated in Figure 1b,
 249 the mechanical scheme of the upgraded model is now composed of four rigid plates
 250 connected by hinges and a single diagonal nonlinear link which governs the in-
 251 plane shear-diagonal mechanism of URM structures. The kinematics associated
 252 with a single spatial panel is described by seven kinematic variables associated
 253 with the rigid body motion and the in-plane shear deformability of the
 254 corresponding masonry panel.

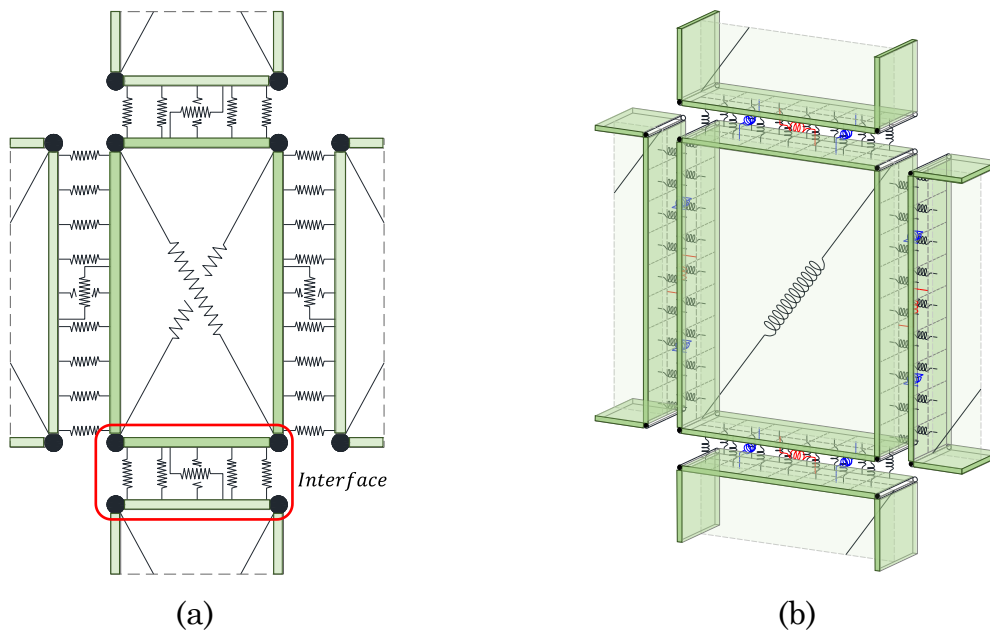


Figure 1. Discrete Macro-Element Modeling approach: (a) two- and (b) three-dimensional mechanical configurations.

255 An accurate simulation of the combined interaction between in-plane and
 256 out-of-plane responses of URM structures requires adequate calibration
 257 procedures for each set of nonlinear links. Different methodologies are followed for
 258 estimating the linear mechanical properties of the links at an interface level and
 259 the diagonal link placed on each panel. The calibration procedure associated with
 260 the transversal and sliding links is based mainly on a fiber approach. Based on
 261 this approach, each adjacent panel is divided into a compound of fibers in
 262 accordance with the discretization of the connecting interface element. Each fiber
 263 represents a strip of masonry in a given direction, and it is characterized by an

264 influence area (A_F for the transversal links, and A_S for the sliding link), and an
 265 equivalent length l . In the case of rectangular elements, the initial flexural
 266 stiffness k_F , related to the transversal links, is reported in equation (1) where
 267 E represents the masonry Young's modulus. The initial stiffness k_S associated
 268 with the sliding response, expressed in equation (2), is defined as a function of the
 269 shear modulus G and a shear factor denoted as α_s whose value ranges between 0
 270 and 1 [36]. This parameter describes the contribution of the in-plane sliding links
 271 and the diagonal link on the overall in-plane elastic shear stiffness of the DME
 272 model. If it presents a value equal to 1, the in-plane sliding links are characterized
 273 by a rigid behavior and the overall in-plane stiffness is given by the diagonal links.
 274 The out-of-plane links contemporary govern the out-of-plane shear and torsion
 275 stiffness of the masonry macro portion simulated by the DME model. The elastic
 276 stiffness of each link is evaluated according to an afference volume associated with
 277 half A_S (Figure 2c). The torsional stiffness is given by equation (3) in which J_ϕ is
 278 the torsional rigidity factor of the panel cross section. In order to reproduce this
 279 stiffness, it is necessary to determine the distance d between the two link which
 280 is reported in equation (4).

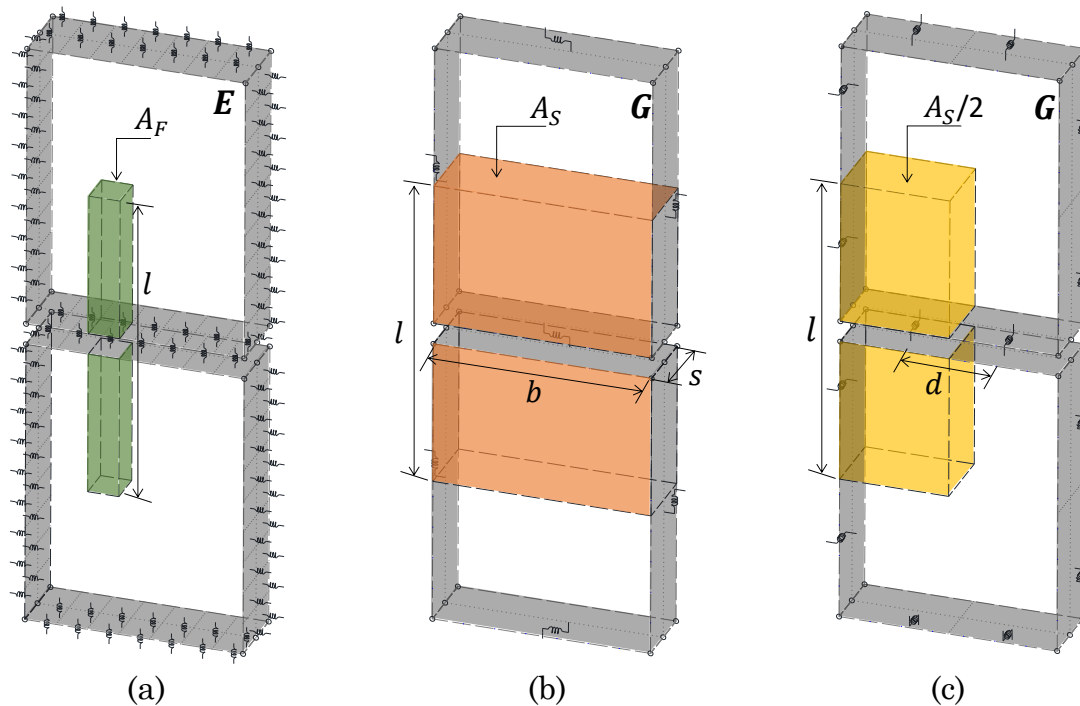


Figure 2. Fiber calibration procedure for: (a) transversal links, (b) in-plane and
 (c) out of plane sliding links.

281

$$k_F = \frac{2EA_F}{l} \quad (1)$$

$$k_s = \frac{GA_s}{l(1-\alpha_s)} \quad (2)$$

$$k_\phi = \frac{G}{l} J_\phi = \frac{G}{l} \left\{ bs^3 \left[\frac{1}{3} - 0,21 \frac{s}{b} \left(1 - \frac{s^4}{12b^4} \right) \right] \right\} = \quad (3)$$

$$d = 2s \sqrt{\frac{1}{3} - 0,21 \frac{s}{b} \left(1 - \frac{s^4}{12b^4} \right)} \quad (4)$$

282 The calibration procedure of the diagonal nonlinear link is conducted by
 283 enforcing an equivalence between a finite portion of masonry with pure shear
 284 deformability, as shown in Figure 3. Based on this equivalence, the shear diagonal
 285 stiffness k_D is given as a function of the shear modulus G , the transversal area A_T ,
 286 the shear factor α_s , the height h , and the angle $\omega = \arctan (h/b)$ described between
 287 the diagonal link and the horizontal edge of the panel. The expression that
 288 describes the initial shear-diagonal stiffness for the spatial panel, illustrated in
 289 Figure 1b, is reported in equation (5) in which V and δ are the shear force and
 290 displacement of the panel, respectively.

$$k_D = \frac{GA_T}{\alpha_s h \cos^2 \omega} \quad (5)$$

291

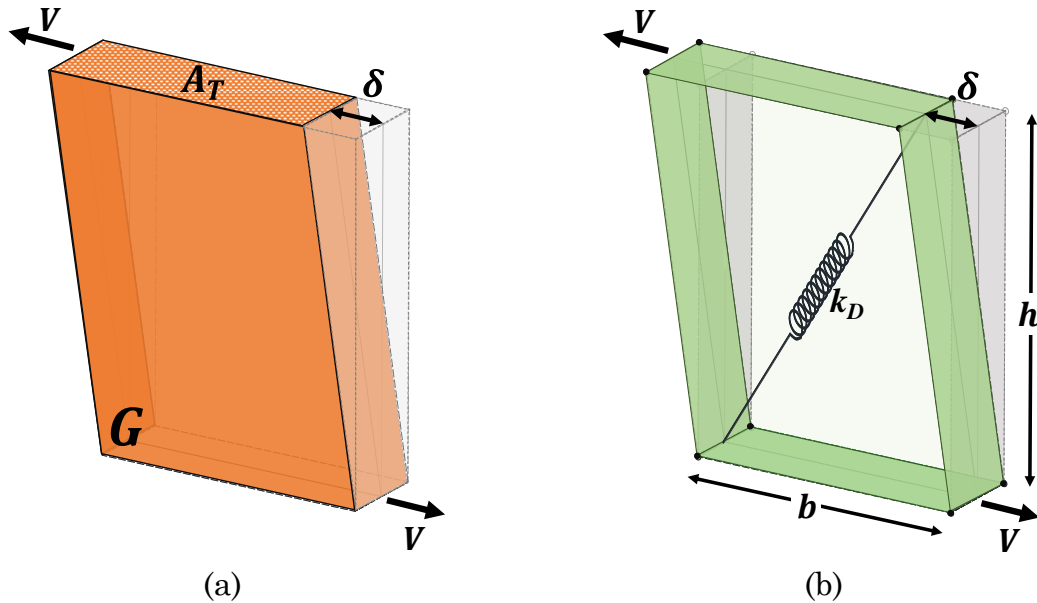


Figure 3. Calibration of diagonal link: (a) finite portion of masonry subjected to pure shear deformation, and (b) rectangular panel.

292 The nonlinear and cyclic behaviors of these links (transversal and sliding)
 293 are characterized by different constitutive models. The nonlinear response of the
 294 transversal links is described by exponential (tension) and parabolic (compression)
 295 constitutive laws. The cyclic behavior of these links corresponds to a hysteretic
 296 Takeda model [37]. Due to the frictional phenomenon of the sliding links, their
 297 nonlinear behavior is described by a Mohr-Coulomb yielding criterion, whereas
 298 the cyclic response of this set of links is associated with an elasto-plastic hysteretic
 299 model. The cyclic constitutive models for these typologies of nonlinear links,
 300 namely the transversal and sliding links, are illustrated in Figure 4 in which F_t
 301 and F_c are the tensile and compression strengths of transversal links (Figure 2a),
 302 whereas F_y corresponds to the ultimate strength sliding links (Figure 2b).

303 Two different yielding criteria can be established for the description of the
 304 post-elastic behavior of the diagonal links. These criteria, named Mohr-Coulomb
 305 and Turnsek and Cacovic [38], take into consideration the confinement condition
 306 to which masonry is subjected for the definition of the shear capacity. The diagonal
 307 nonlinear links are also characterized by a cyclic response governed by a Takeda
 308 hysteretic model [37] in which the unloading cycles recover the initial stiffness.
 309 The cyclic constitutive model for the nonlinear diagonal link is illustrated in
 310 Figure 4c in which F_v corresponds to its ultimate strength. Further details
 311 regarding the calibration procedure and the cyclic behavior of these sets of links
 312 are reported in [39]. The proposed modeling approach has been implemented in
 313 the structural code HiStrA (Historical Structure Analysis) software [40].

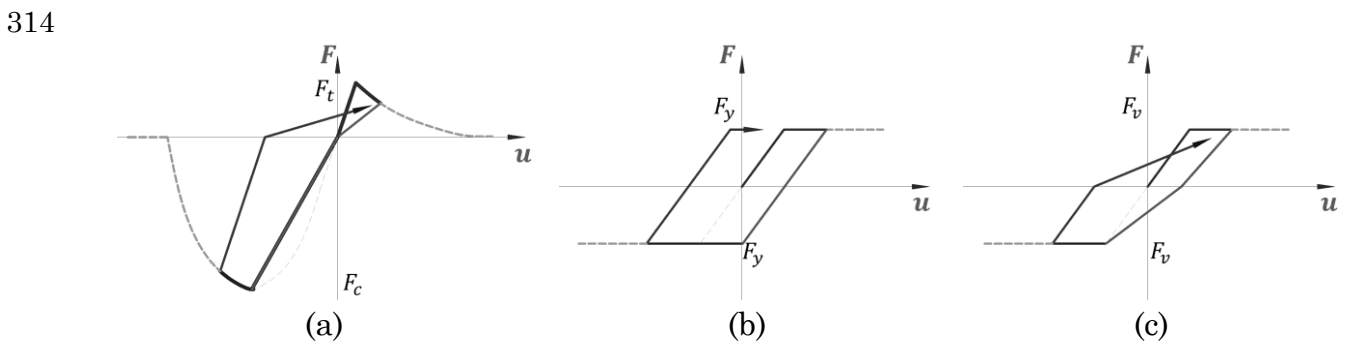


Figure 4. Constitutive models and hysteretic behavior of the different typologies of nonlinear links: (a) transversal, (b) sliding, and (c) diagonal.

315 **3. Proposed procedure for seismic vulnerability** 316 **assessment**

317 Seismic vulnerability assessment is often conducted by means of analytical
318 fragility functions which are capable of providing the probability of a structure to
319 reach or exceed a LS due to a given IM. A fragility curve can be described by a
320 normal cumulative distribution function Φ , which is characterized by a mean
321 value θ and a standard deviation β as reported in equation (6). In most
322 investigations associated with masonry structures, the derivation of fragility
323 curves usually involves the application of nonlinear static analyses using
324 simplified numerical tools aiming at reducing the computational demand. Several
325 of these formulations are based on overly simplified numerical models neglecting
326 some relevant aspects of URM structures such as the occurrence of out-of-plane
327 mechanisms. Aiming at obtaining more realistic results, this investigation
328 proposes a different methodology for the assessment of URM buildings which
329 involves the use of nonlinear static and dynamic analyses performed by means of
330 the discrete macro-element method previously introduced.

$$P(LS|IM = x) = \Phi\left(\frac{\ln(x/\theta)}{\beta}\right) \quad (6)$$

331 The procedure for the seismic vulnerability assessment of URM structures
332 presented in this paper involves three main activities: i) definition of seismic
333 input, ii) definition of adequate LSs and their corresponding capacity, and
334 iii) derivation and fitting of the fragility curves. Since the proposed modeling
335 approach is characterized by a reduced number of DOFs, and therefore a low
336 computational demand, the seismic vulnerability assessment is performed by
337 nonlinear static and dynamic analyses. In this sense, it is necessary to define
338 proper seismic accelerograms, consistent with the design spectra, which can be
339 associated with real ground motion records as well as synthetic or artificial
340 accelerograms (first activity). Here, accelerograms artificially generated, following
341 specifications reported in standards, have been adopted.

342 For the definition of accurate capacities for the selected LSs (second
343 activity), a novel approach, based on multidirectional pushover analyses, is

344 proposed. This approach involves the application of a set of nonlinear static
 345 analyses, along different directions, with an incremental angular step as reported
 346 by Cannizzaro, et al. [41]. The result, denoted as *Capacity Dominium* (CD), allows
 347 the definition the displacement capacity as a function of the direction of the input
 348 for each defined LS. It is worth to note that, based on this alternative approach,
 349 different displacement-based criteria can be used for the definition of the LSs.

350 The derivation of the fragility curves (third activity), implies the
 351 introduction of uncertainty in the numerical model. In this investigation, the
 352 uncertainty is associated with the seismic input (scaled artificial accelerograms)
 353 and with other parameters such as mechanical properties or geometric
 354 configurations. This last activity also involved a fitting procedure for the
 355 estimation of the true probability, which considers the total number of analyses
 356 and the ones that led to the exceedance of the LS. As reported by Baker [42], a
 357 fitting process is given by a maximum likelihood approach aiming at optimizing
 358 the mean value θ and standard deviation β that characterize the fragility function.
 359 The true probability P of exceeding a LS due to the j^{th} IM is given by the binomial
 360 distribution p reported in equation (7) in which z and n correspond, respectively,
 361 to the total and exceeding number of nonlinear dynamic analyses, denoted as
 362 events hereafter. The likelihood function can be computed as the product of the
 363 binomial distributions associated with the different m levels of IMs, as reported in
 364 equation (8). The fitting procedure consisted of estimating the optimum values of
 365 θ and β , which provide the maximum likelihood.

$$P(z_j \text{ collapse in } n_j \text{ events}) = \binom{n_j}{z_j} p_j^{z_j} (1-p_j)^{n_j-z_j} \quad (7)$$

$$Likelihood = \prod_{j=1}^m \binom{n_j}{z_j} \Phi\left(\frac{\ln(x_j/\theta)}{\beta}\right)^{z_j} \left(1 - \Phi\left(\frac{\ln(x_j/\theta)}{\beta}\right)\right)^{n_j-z_j} \quad (8)$$

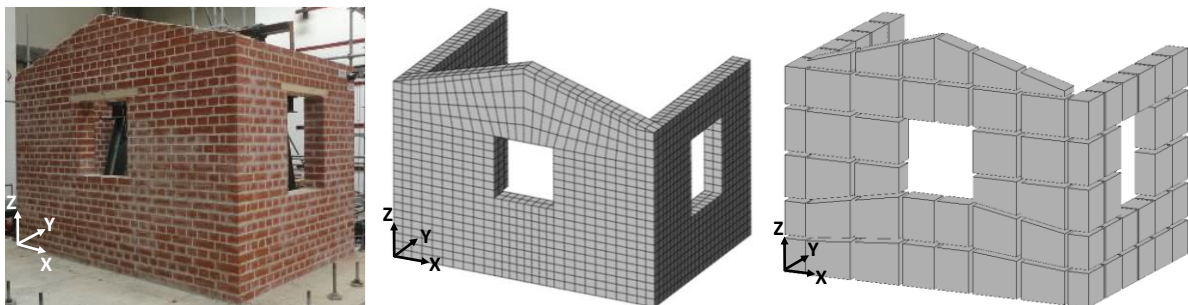
366 The proposed methodology presents two novel contributions, namely, the
 367 application of multidirectional pushover analysis for the definition of the
 368 displacement capacity, and the application of extensive nonlinear dynamic
 369 analyses for the derivation of fragility curves when considering more detailed
 370 numerical models capable of considering the interaction between in-plane and out-

371 of-plane mechanisms. Firstly, the CD allows a proper identification of LSs since it
372 can be combined with different LSs criteria, and it can also be applied to any
373 structural typology. Secondly, time history analysis constitutes a more precise tool
374 for the assessment of the seismic response of structures since it involves energy
375 dissipation as well as the degradation of strength and stiffness of the material.

376 **4. Application to a brick masonry structure**

377 The proposed procedure for the seismic vulnerability assessment of URM
378 structures was applied to a brick specimen characterized by a strong out-of-plane
379 collapse mechanism. The seismic response of such masonry structure was
380 thoroughly investigated by means of shaking table tests [43] as well as numerical
381 simulations [39] according to a deterministic approach. The case study and the
382 main results previously obtained are here briefly recalled. As depicted in Figure
383 5a, the considered U-shape structure was composed of three walls: a main gable
384 and two return walls with an equal thickness of 0.235 m. The base of the main
385 gable wall was equal to 3.50 m whereas its height presented a value of 2.75 m at
386 the top of the tympanum. The base and height of both return walls were equal to
387 2.25 m and 2.50 m, respectively. This URM structure also presented two window
388 openings: one at the main gable wall and another one at one return wall with
389 dimensions of 0.80 x 0.80 m² and 0.80 x 1.00 m², respectively. The unusual
390 geometry of the prototype, characterized by a U-shape plan layout, was chosen
391 with the aim to investigate the behavior of the main gable wall taking into account
392 the possible constraining effect of typical return walls. The brick masonry
393 structure was subjected to the 2011 Christchurch earthquake which was applied
394 in the direction perpendicular to the main gable wall (Y-direction in Figure 5a).
395 As reported in [43], the experimental campaign consisted of eight shaking table
396 tests in which the ground motion was amplified by scaling factors until the
397 structure reached collapse. The out-of-plane behavior of the structure was also
398 investigated by means of two numerical approaches, namely FE and Discrete
399 Macro-Element (DME) models characterized by a different discretization, as
400 illustrated in Figure 5b and Figure 5c respectively. The FE model was built using
401 the DIANA software [44], and it was characterized by a rotation total strain crack

402 model. The element type used for the FE model consisted of twenty-node bricks
 403 CHX60 which were described by a 3x3x3 integration scheme [44]. On the other
 404 hand, the DME model was implemented by means of the HiStrA software [40],
 405 using the constitutive laws for the nonlinear links presented in Section 2. These
 406 numerical models presented a great difference in terms of DOFs: 54477 for the FE
 407 model, and 616 for the DME model. Both models were subjected to static and
 408 dynamic nonlinear analyses for investigating the out-of-plane response of the
 409 main gable wall. Mass proportional pushover analyses and nonlinear dynamic,
 410 consistent with the last seismic input recorded during the shaking table tests (see
 411 Figure 5f), have been applied in the direction perpendicular to the main gable wall
 412 (Y-direction in Figure 5b-c). Figure 5d shows the significant agreement between
 413 the two modeling approaches when performing pushover analyses, especially in
 414 the negative direction (-Y). It can be noted that there is a good agreement in
 415 maximum capacity in the +Y-direction, but the residual forces of these two
 416 modelling approaches are somehow different due to their corresponding failure
 417 mechanisms. In the case of the FE model, the collapse is governed by in-plane and
 418 out-of-plane mechanisms, whereas, in the case of the DME model, the response is
 419 centered on the main gable wall. The comparison in terms of time history analyses
 420 is depicted in Figure 5e demonstrating the capability of the proposed modeling
 421 approach of providing a satisfactory simulation of the dynamic response of a
 422 sophisticated model with a strongly reduced computational burden (96%). The
 423 duration of the nonlinear dynamic analysis associated with a FE model was
 424 approximately [39], Figure 5g[39].



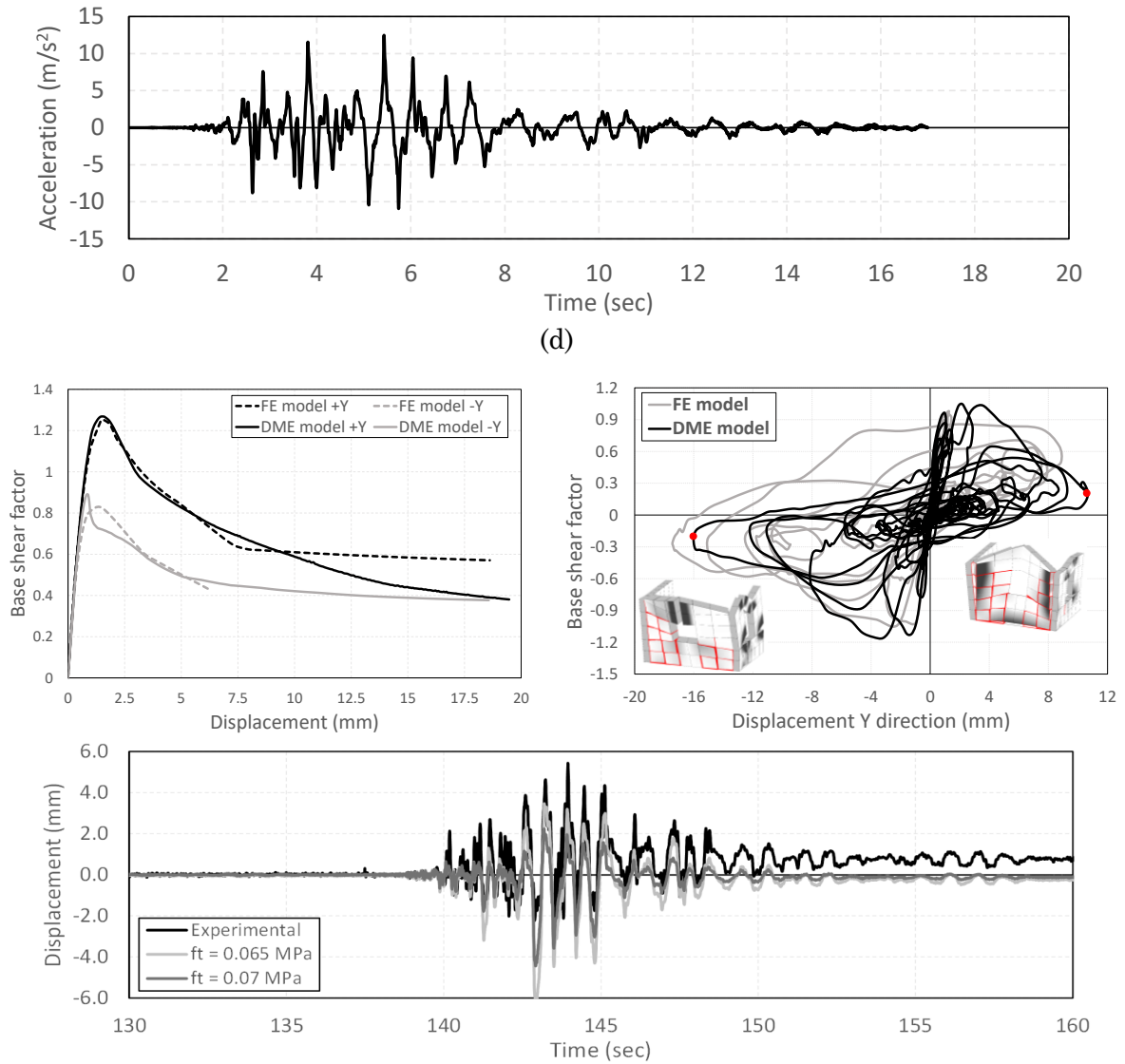
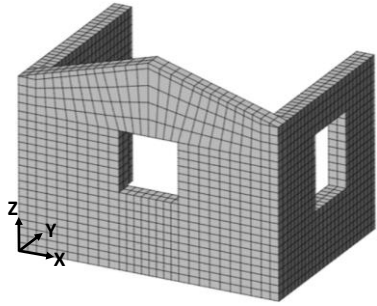


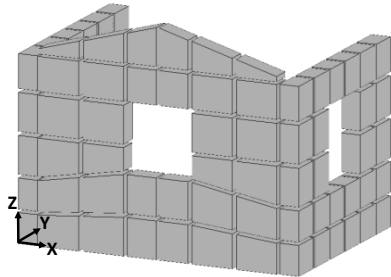
Figure 5. Brick masonry structure: (a) benchmark, (b) FE and, (c) DME models, (d) seismic input, comparison in terms of (e) pushover curves, and (f) hysteretic response, and (g) experimental and numerical history of displacement due to the application of seventh ground motion [39].



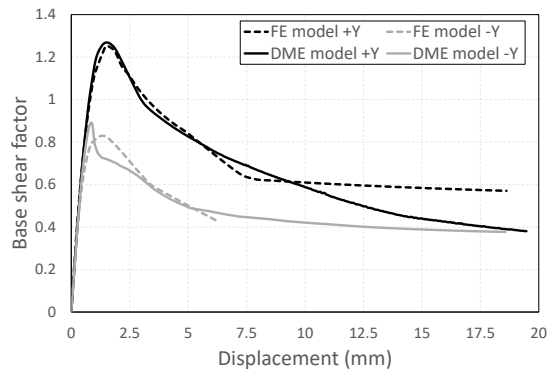
(a)



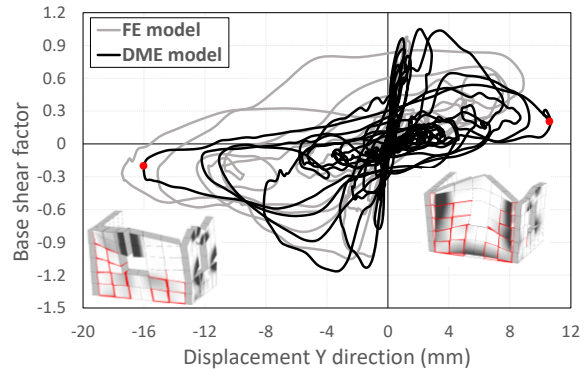
(b)



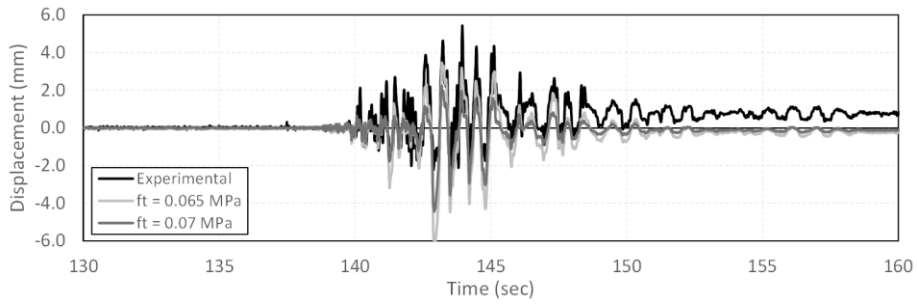
(c)



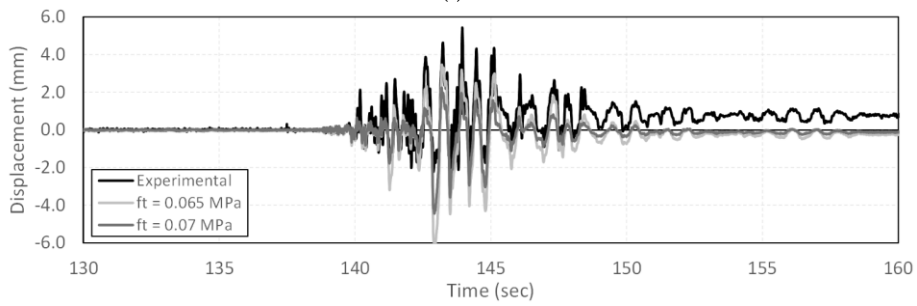
(d)



(e)



(f)



(g)

426 4.1. Step 1: Definition of seismic input

427 Aiming at assessing the seismic vulnerability of the considered brick
 428 masonry structure, nonlinear dynamic analyses, performed on the DME model,
 429 have been based on uniaxial as well as three-component artificial accelerograms.
 430 The uniaxial seismic inputs have been applied in the direction perpendicular to
 431 the main gable wall in order to investigate its out-of-plane response when the
 432 excitation acts in the orthogonal direction only. The three-component artificial
 433 accelerograms have been applied to the structure to investigate the response of
 434 the gable walls under in-plane, out-of-plane and vertical base acceleration
 435 components. The artificial accelerograms were generated so that they match the
 436 horizontal and vertical elastic response spectra with 5% of viscous damping as
 437 specified by the EC8-Part1 [45]. Type 1 and Type 2 elastic response spectra,
 438 respectively associated with far- and near-field seismic inputs, were taken into
 439 consideration for this investigation. The horizontal $S_{he}(T)$ and vertical $S_{ve}(T)$
 440 components of these spectra are illustrated in Figure 6, and their definition is
 441 given in [45].

442 The generation of the artificial accelerograms was conducted considering
 443 a reference horizontal design ground acceleration a_g equal to 1 g and 5% of viscous
 444 damping ($\eta = 1$). Assuming that the brick masonry structure was located in a
 445 Lisbon area, the soil factor S was established as 1, which corresponds to a class A
 446 soil (rigid soil). The reference spectrum periods T_B , T_C and T_D were established
 447 considering the Portuguese National Annex [46]. This code also provides a ratio
 448 between vertical (a_{vg}) and horizontal (a_g) design ground accelerations. The
 449 different parameters required for the definition of the elastic response spectra
 450 Type 1 (far-field earthquakes) and Type 2 (near-field earthquakes) are
 451 summarized in Table 1.

Table 1. Parameters for the definition of horizontal elastic response spectrum.

Component	Elastic response spectrum	Soil type	S	a_{vg} (g)	H	T_B (sec)	T_C (sec)	T_D (sec)
Horizontal	Type 1	A	1	-	1	0.10	0.60	2.00
	Type 2	A	1	-	1	0.10	0.25	2.00
Vertical	Type 1	-	-	$0.75 a_g$	1	0.05	0.25	1.00
	Type 2	-	-	$0.95 a_g$	1	0.05	0.15	1.00

452

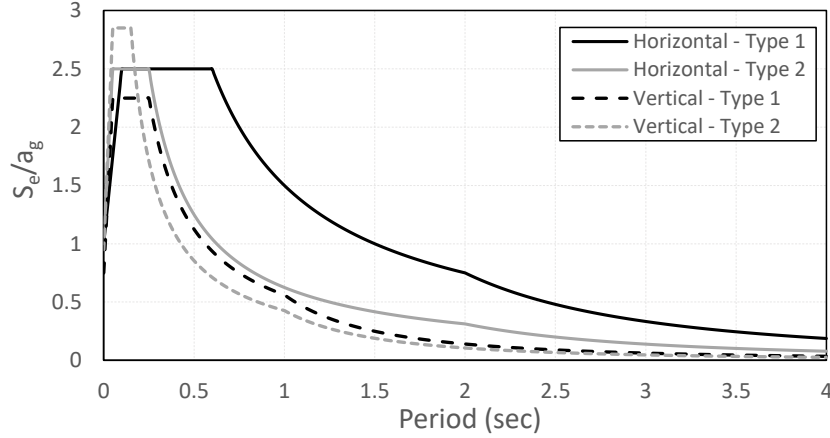


Figure 6. Elastic response spectra used for the generation of artificial accelerograms.

453 In addition to the elastic response spectra, the generation of artificial
454 seismic input also required the definition of minimum duration of stationary part
455 of acceleration. In accordance with the Portuguese National Annex [46], far- and
456 near-field based artificial accelerograms are characterized by stationary times of
457 30 sec and 10 sec, respectively. In this sense, the artificial accelerograms were
458 generated considering total durations of 40 sec for far-field earthquakes and 20 sec
459 for near-field earthquakes. The generation of artificial accelerograms was
460 conducted using the software SIMQKE [47]. An initial set of 1200 horizontal and
461 600 vertical samples were generated between Type 1 and Type 2 earthquakes.
462 Since both horizontal components need to be uncorrelated, their generation was
463 conducted separately. The accuracy of this initial set was assessed by the
464 comparison between the spectrum of each accelerogram and the elastic response
465 spectrum used for its generation. The artificial accelerograms whose spectrum
466 lacked resemblance with its corresponding elastic response spectrum were
467 discarded from the initial set. The selection of suitable samples led to a final set of
468 560 horizontal and 280 vertical artificial accelerograms which were subsequently
469 subjected to a baseline correction by means of the software LNEC-SPA [48]. A high
470 pass Fourier filter of 0.20 Hz and a cosine-based windowing approach were
471 considered for the signal processing of the accelerograms.

472 4.2. *Step 2: Definition of displacement capacity*

473 The definition of appropriate limit states LSs constitutes a relevant task
474 for seismic vulnerability assessment. The LSs can be evaluated considering the
475 capacity of a structure in terms of interstory drift, damaged area, hysteretic
476 energy or base-shear resistance. From the different approaches, the assessment of
477 the seismic vulnerability of masonry structures is usually conducted based on
478 interstory drift procedures. For instance, the EC8-Part3 [9] establishes three LSs,
479 namely Damage Limitation, Significant Damage and Near Collapse, together with
480 their corresponding displacement capacity. The capacity associated with the first
481 LS is given by the yielding displacement, whereas the definition of the capacity
482 related to the second LS depends on the type of failure mechanism, namely
483 flexural and shear. The capacity of the remaining LS (Near Collapse) is defined as
484 $\frac{4}{3}$ of the drift associated with a Significant Damage LS. Nevertheless, the
485 definition of these interstory drift capacities is related to masonry structures with
486 a box-type behavior; and therefore, they are not suitable for structures with
487 predominant out-of-plane collapse mechanisms. The multiscale approach
488 proposed in [17, 18] may be considered as a proper formulation for the definition
489 of LSs of the masonry structure under investigation; however, due to its
490 predominant out-of-plane behavior as well as its irregular geometrical
491 characteristics, it was decided to adopt an alternative procedure. In this regard,
492 the CD constitutes a tool that enables the evaluation of the global response of the
493 structure allowing a comprehensive representation of the capacity of the building
494 and a proper identification of LSs.

495 The EC8-Part3 [9] and the Italian Code [11] relate the definition of LSs to
496 the base shear of the structure. These LSs, namely Near Collapse for the former
497 and Life Safety for the latter, are established when a structure experiences a 20%
498 loss of its maximum shear resistance (ultimate displacement). For the proposed
499 methodology, such shear capacity based formulation was taken into consideration
500 for the definition of two of the LSs, namely Near Collapse and Significant Damage.
501 The definition of the first LS (Damage Limitation) was given by the yielding
502 displacement as specified in the EC8-Part 3 [9]. A summary of the LSs used in this

503 investigation, together with their corresponding displacement capacity, is
 504 reported in Table 2.

Table 2. Limit states and displacement capacity for the assessment of the seismic vulnerability of the brick masonry structure.

Limit State	Capacity definition
Damage Limitation	u_y (yielding displacement)
Significant Damage	$3(u_u)/4$
Near Collapse	u_u (ultimate displacement at 20% reduction of base shear capacity)

505 In the proposed methodology, the definition of the displacement capacity
 506 of the LSs involves the application of an alternative procedure denoted as *Capacity*
 507 *Dominium* (CD) [49]. In this procedure, the structure is subjected to a set of
 508 nonlinear static analyses along different angles aiming at assessing its global
 509 response. For this investigation, the brick masonry structure was subjected to a
 510 set of sixteen analyses with an incremental angular step of 22.5° as illustrated in
 511 Figure 7. These analyses were performed by applying an incremental force
 512 proportional to the mass in each direction. The mechanical properties of the DME
 513 model were adopted according to [39] which are reported as the mean values in
 514 Table 3. The global response of the structure was evaluated by considering the
 515 control nodes with highest out-of-plane displacements: one located at the top of
 516 the tympanum and two placed at the top of the end of both return walls.

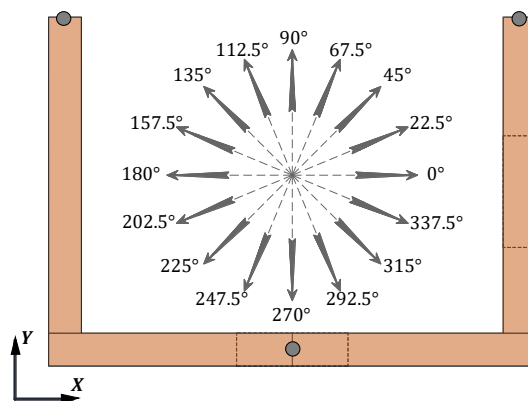
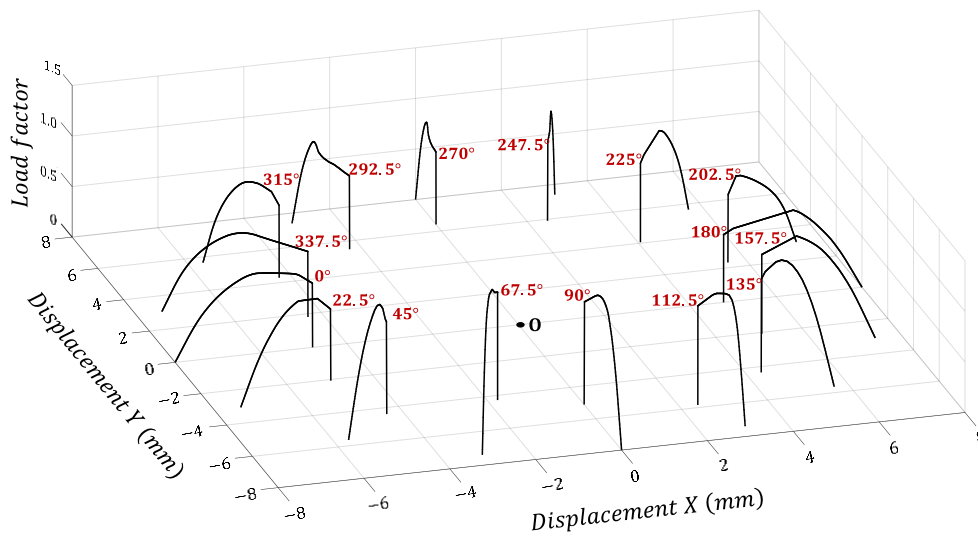


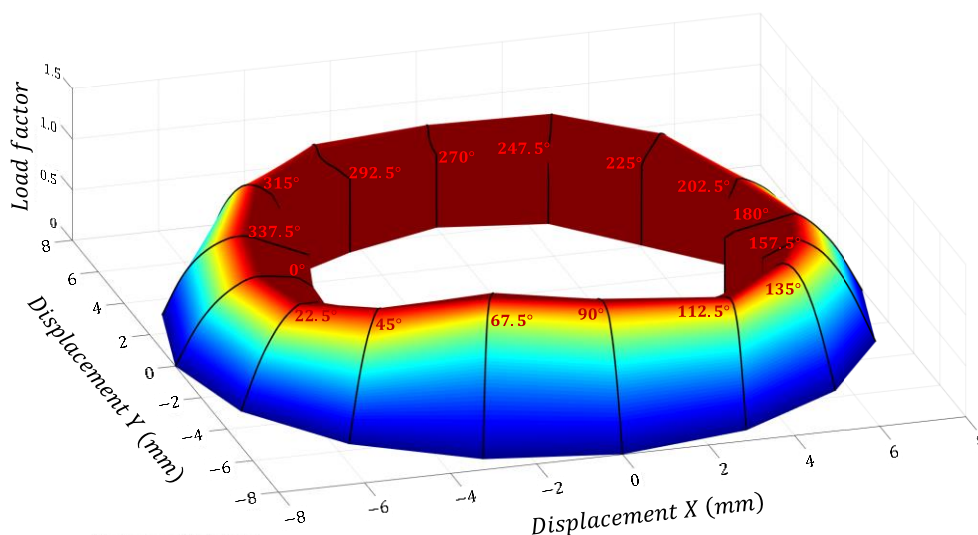
Figure 7. Application of nonlinear static analyses for the definition of the LSs based on a Capacity Dominium procedure.

517 The CD for a Near Collapse LS was built taking into consideration the
 518 sixteen pushover curves until a 20% loss of maximum shear capacity was attained.

519 As illustrated in Figure 8a, the pushover curves were plotted backward, along
 520 their corresponding angles, and at an equal distance of 8 mm from the origin **O**.
 521 Subsequently, patches were employed to connect each pushover curves aiming at
 522 the definition of a color map basket domain (see Figure 8b) which corresponds to
 523 a three-dimensional representation of the global capacity of the brick masonry
 524 prototype. In Figure 8, the vertical axis is associated with the load factor (ratio
 525 between base shear and self-weight), whereas the horizontal axes are related to
 526 the horizontal displacements in X and Y directions, respectively.



(a)



(b)

Figure 8. Construction of basket domain based on the application of pushover analyses along different angles: (a) multidirectional pushover curves, and (b) three dimensional basket domain.

527 The CD associated with the Near Collapse LS can be determined as the
528 effective displacement field in the three-dimensional basket domain as shown in
529 the gray area in Figure 9a. Such displacement field is created by connecting a set
530 of nodes in accordance with the different pushover curves and their corresponding
531 angle plotted in the three-dimensional basket domain. These contouring nodes are
532 located at a distance d_a equal to the ultimate horizontal displacement from the
533 origin O. Following a similar approach and considering the specifications provided
534 by the EC8-Part3 [9], the CD for the two additional LSs were also properly
535 established. In the case of the Damage Limitation LS, the displacement field was
536 associated with the yielding displacement and it is given by the blue area in Figure
537 9b. The CD for a Significant Damage LS was defined as a ratio of 3/4 with respect
538 to the Near Collapse LS (red area in Figure 9b) as stated by the EC8-Part3 [9]. It
539 is remarkable how the CDs change shape as a function of the LS. As an example,
540 the +X/-Y sector is rather stringent in terms of Damage Limitation LS, while the
541 -X/-Y sector becomes rather stringent for the Significant Damage and Near
542 Collapse LSs, when compared with the remaining LSs in the same sector. This
543 behavior can be associated with the presence of a window opening in one return
544 wall which introduces asymmetry to the structure. In addition, it is possible to
545 notice that different shapes of the CDs in the -Y and +Y sectors. These different
546 shapes are given by the asymmetry generated by the window openings but also by
547 the influence of the return walls on the global stiffnesses of the structure and their
548 capacity to deform.

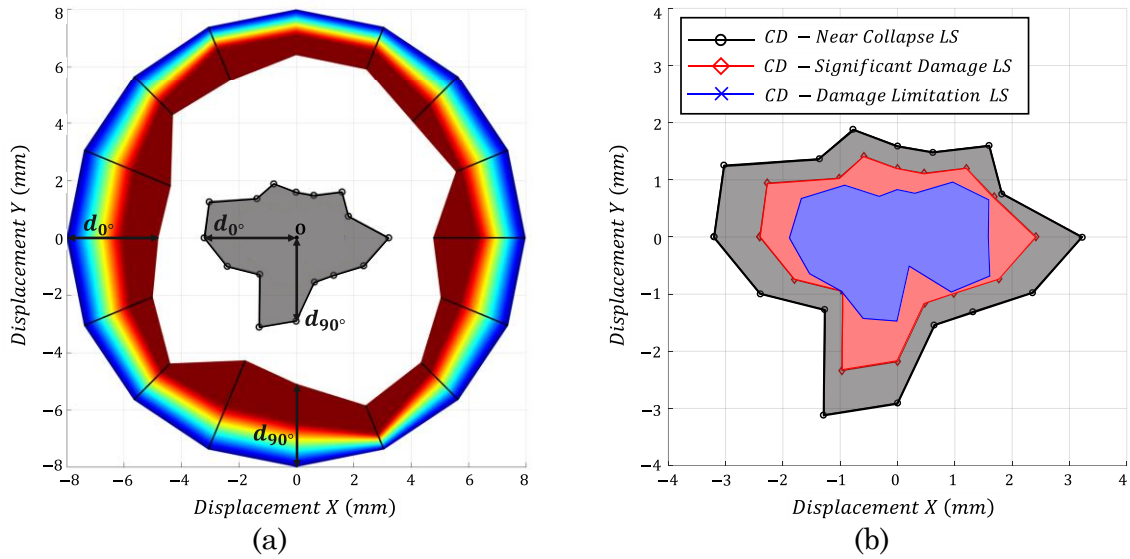


Figure 9. Displacement capacity: (a) creation of effective displacement field, and (b) Capacity Dominium for the selected LSs.

549 4.3. Step 3: Derivation and fitting of analytical fragility curves

550 In this work, the seismic vulnerability of the masonry structure was
551 assessed by the derivation of analytical fragility curves through the application of
552 nonlinear dynamic analyses. For this purpose, the DME model of this prototype
553 was subjected to artificial accelerograms compatible with the design spectra.
554 Although the generation of the seismic input constitutes a significant source of
555 uncertainty, it is necessary to consider different sources of uncertainty in order to
556 conduct a more reliable seismic vulnerability assessment. These additional
557 uncertainties have been mainly focused on mechanical properties which require
558 the definition of probability density functions (PDFs) together with mean values
559 and coefficients of variation (COVs). The mean values and COVs of material
560 properties such as Young's modulus E , specific weight γ , compressive f_c , and tensile
561 f_t strength, were established based on the mechanical characterization conducted
562 by Candeias, et al. [43]. In such investigation, simple and diagonal compression
563 tests were conducted to the brick masonry in order to determine the latter
564 mechanical properties as well as their statistical characteristics. The mean values
565 of other mechanical properties, namely, tensile fracture energy G_f^I , shear modulus
566 G , shear strength f_{y0} , cohesion c , and friction coefficients associated with the
567 diagonal and sliding failure modes (μ_d and μ_s), were defined as the parameters
568 presented in the seismic assessment of the brick masonry structure conducted in

569 [39]. On the other hand, the mean values of the fracture energies in compression
570 G_c and shear-sliding G_f^H , were given as a function of ductility indexes as reported
571 in literature. For instance, Lourenço [50] provided average values for ductility
572 indexes in compression d_{uc} and shear-sliding d_{us} equal to 1.6 mm and 0.09 mm,
573 respectively. The definition of COVs for the mechanical properties associated with
574 the shear mechanisms (diagonal and sliding) followed the specifications provided
575 by the JCSS Probability Model Code [51]. In the case of shear strength and
576 cohesion, the COV presented a value of 40%, whereas, in the case of friction
577 coefficients, this value was equal to 19%. Due to the lack of information related to
578 the remaining mechanical properties, it was assumed that their corresponding
579 COVs corresponded to 30%. The statistical characteristics for the mechanical
580 properties are summarized in Table 3. In this investigation, the uncertainty was
581 also focused on other geometrical and structural parameters such as thickness and
582 viscous damping ratio. In the case of the wall thickness, a mean value of 23.5 cm
583 and a COV of 5% were established as statistical characteristics. The viscous
584 damping ratio presented a mean value of 3%, and due to the lack of information
585 associated with this structural parameter for URM structures, it was assumed
586 that it presented a COV of 30%. It is worth to note that the different uncertain
587 parameters (mechanical, geometrical and structural) were characterized by a
588 lognormal PDF.

Table 3. Probabilistic models associated with the mechanical properties of the DME model.

	Parameter		Mean	COV
Elastic behavior	Young's modulus	E N/mm ²	5170	29%
	Shear modulus	G N/mm ²	2133	30%
	Specific weight	γ N/mm ³	18.9x10 ⁻⁶	3%
Tensile behavior	Tensile strength	f_t N/mm ²	0.1	19%
	Fracture energy	G_f^I N/mm	0.012	30%
Compressive behavior	Compressive strength	f_c N/mm ²	2.48	14%
	Compressive ductility index	d_{uc} mm	1.6	30%
Shear-sliding behavior	Cohesion	c N/mm ²	0.1	40%
	Friction coefficient	μ_s -	0.7	19%
	Shear-sliding ductility index	d_{us} mm	0.09	30%
	Shear strength	f_{y0} N/mm ²	0.07	40%

Shear- diagonal behavior	Friction coefficient	μ_d	-	0.6	19%
--------------------------------	----------------------	---------	---	-----	-----

589 The seismic vulnerability of the brick masonry structure was initially
590 evaluated through the application of a set of 2000 time-history analyses based on
591 uniaxial artificial accelerograms (along the Y direction, perpendicular to the main
592 gable wall). From this initial set, 1000 analyses were associated with far-field
593 seismic input (Type 1), whereas the remaining 1000 were related to near-field
594 seismic input (Type 2). Each of these sets was subsequently divided into eight
595 groups of 125 analyses in order to consider different intensity levels of PGA. Since
596 the artificial accelerograms were generated with a horizontal design acceleration
597 equal to 1 g, it was necessary to scale them aiming at comprising a wide range of
598 PGA. In this case, eight scaling factors ranging between 0.45 and 0.80 (with an
599 incremental step of 0.05) were defined for the seismic vulnerability assessment of
600 the brick masonry structure. In order to define the uniaxial seismic inputs,
601 125 horizontal components were randomly selected from the corresponding final
602 set of artificial accelerograms generated in Section 4.1. Subsequently, 125 random
603 values of the different uncertain geometrical and mechanical parameters were
604 defined based on their corresponding mean value, COV, and PDF. It is worth
605 noting that the computational demand required for the assessment of the seismic
606 vulnerability assessment of this structure was acceptable since the average
607 duration of a single analysis was about 30 minutes using a conventional desktop.

608 An automatic routine was implemented for the application of time history
609 analyses considering the variability of seismic inputs and uncertain parameters.
610 The structural damping was assigned based on a Rayleigh criterion by considering
611 natural frequencies of 18.8 Hz and 75.4 Hz as reported in [39]. These values were
612 obtained after an eigenvalue analysis considering the mean values of the initial
613 mechanical properties, and they remained constant despite the variation of
614 properties such as the Young's modulus since it would require additional
615 computational burden for the estimation of the dynamic properties for each time
616 history analysis. Moreover, it is worth noticing that the contribution of viscous
617 damping can be considered negligible if compared to the hysteretic dissipation
618 considering the high non-linearity characterizing the structural response. The

619 definition of the mass properties of the numerical model was based on an efficient
620 diagonal mass matrix as reported in [52].

621 The CD related to each LSs, introduced in the previous sub-section, has
622 been obtained by analyzing the nonlinear response of the prototype when
623 subjected to static loading. The identification of the exceedance of a certain LS
624 when the structure is subjected to dynamic loading is not straightforward since
625 the displacement capacity of a structure subjected to earthquake dynamic loading
626 is generally higher, when compared to the corresponding capacity obtained for a
627 monotonic application of horizontal static loads. For this reason, it is necessary to
628 establish a conventional criterion for the exceedance of each LS. In the application
629 here performed in order to conduct the maximum likelihood fitting process, it has
630 been assumed that an exceeding event is given when the history of the horizontal
631 top displacements exceeds the area of its corresponding CD at least twice (a single
632 event is disregarded, while a second event is assumed as a confirmation. Initially,
633 the seismic vulnerability assessment was carried out considering that an event
634 exceeded a given LS when the dynamic response surpassed the CD at least once.
635 However, a single time could be considered as an impact or outlier caused by the
636 seismic input and not as the real collapse of the structure. Therefore, the events
637 in which the dynamic response remained inside the CD or surpassed only once the
638 displacement field were not included in the fitting procedure.

639 The assessment of the dynamic response due to the application of Type 2
640 uniaxial seismic input is illustrated throughout Figure 10 for the three LSs
641 defined for this investigation. In this figure, the responses associated with each of
642 the three control nodes selected for the definition of the CD were plotted together.
643 As it was expected, the dynamic response of the numerical model was strongly
644 characterized by histories of displacements in the Y direction (node at the top of
645 the main gable wall), since the seismic input was applied only in that direction.
646 The response of the other two control nodes did not present a significant
647 displacement since the dynamic load was applied in one direction. The assessment
648 was focused on the out-of-plane behavior of the façade; therefore, only the results
649 associated with the top of the tympanum as control node were considered for the

650 assessment of the seismic vulnerability of this structure. The number of exceeding
 651 events out of the 125 set of accelerograms are summarized in Table 4.

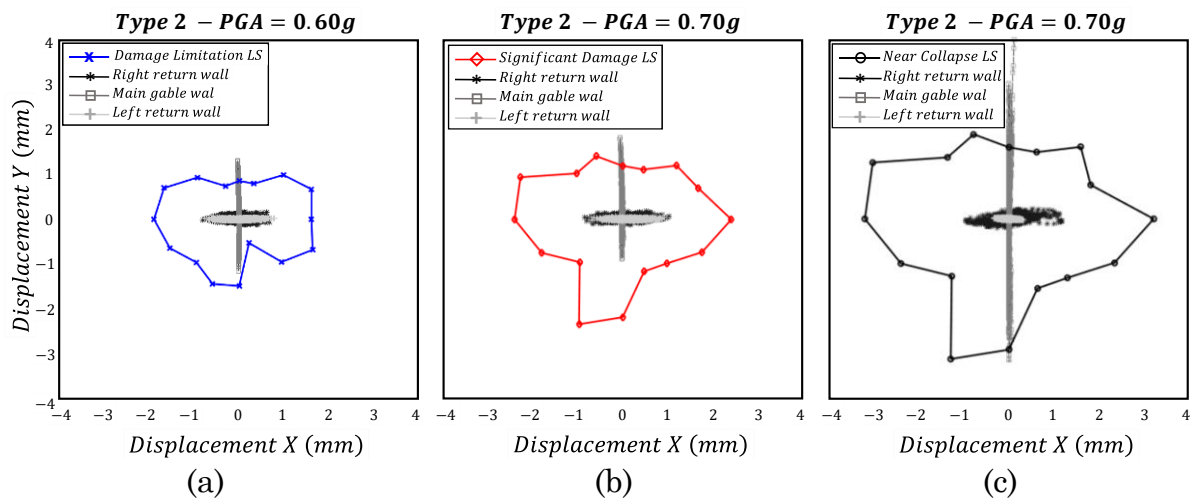


Figure 10. Assessment of seismic performance based on a Capacity Dominium due to the application of uniaxial artificial accelerograms to different LSs: (a) Damage Limitation , (b) Significant Damage, and (c) Near Collapse.

652

Table 4. Exceeding events for the derivation of analytical fragility curves due to the application of uniaxial artificial accelerograms (out of a set of 125).

IM	Number of events	Number of exceeding events					
		Damage Limitation LS		Significant Damage LS		Near Collapse LS	
		Type 1	Type 2	Type 1	Type 2	Type 1	Type 2
0.45 g	125	32	27	19	26	13	6
0.50 g	125	51	35	28	55	26	14
0.55 g	125	81	50	37	79	48	24
0.60 g	125	96	74	57	89	62	42
0.65 g	125	106	92	73	106	79	59
0.70 g	125	116	102	92	110	92	72
0.75 g	125	122	110	99	116	108	91
0.80 g	125	123	115	110	120	112	99

653 The fitted analytical fragility curves obtained from the application of
 654 uniaxial artificial accelerograms are illustrated in Figure 11. From these results,
 655 it is possible to determine the probability of exceedance of a LS due to the
 656 occurrence of a seismic event with a given value of PGA. In the case of far-field
 657 earthquakes, there is a 44% of probability of exceeding the Damage Limitation LS
 658 when the brick masonry structure is subjected to a seismic intensity of 0.50 g (see
 659 solid lines in Figure 11). This probability reduces to 31% and 22% when
 660 considering the Significant Damage and Near Collapse LSs, respectively. In a
 661 similar way, it is also possible to estimate the expected seismic intensity in terms
 662 of PGA for a desired probability of exceedance. For instance, the Damage

663 Limitation LS is exceeded with a probability of 50% when the PGA of the seismic
664 input corresponds to approximately 0.52 g. In the case of the remaining LSs, the
665 expected intensity of the uniaxial seismic input increases to 0.57 g and 0.61 g. It
666 was also observed that the analytical fragility curves of the different LSs obtained
667 from the application of uniaxial far-field seismic inputs were not so separated.
668 Such behavior is strictly related to the characteristics of the CD and the definition
669 of the capacity of the LSs since the displacement fields were close to each other as
670 a result of the rapid loss of shear resistance and the quasi-brittle behavior of the
671 material, as a consequence of the low-ductility capacity of the structure. The
672 dashed lines in Figure 11 illustrate the analytical fragility curves associated with
673 the application of near-field seismic input. In this case, the probabilities of
674 exceedance of the different LSs were also estimated considering a seismic intensity
675 of 0.50 g. For a Damage limitation LS, this probability corresponds to 42% which
676 is slightly lower when comparing it to the one obtained with far-field seismic
677 inputs. A stronger reduction was observed for the Significant Damage and Near
678 Collapse LSs. In the former, the probability of exceedance presents a value of 22%,
679 whereas, in the latter, such probability corresponds to 11%. In these cases, the
680 reduction between far- and near-field probabilities is around 10%, and it may also
681 be related to the characteristics of the seismic input such as frequency content and
682 stationary time.

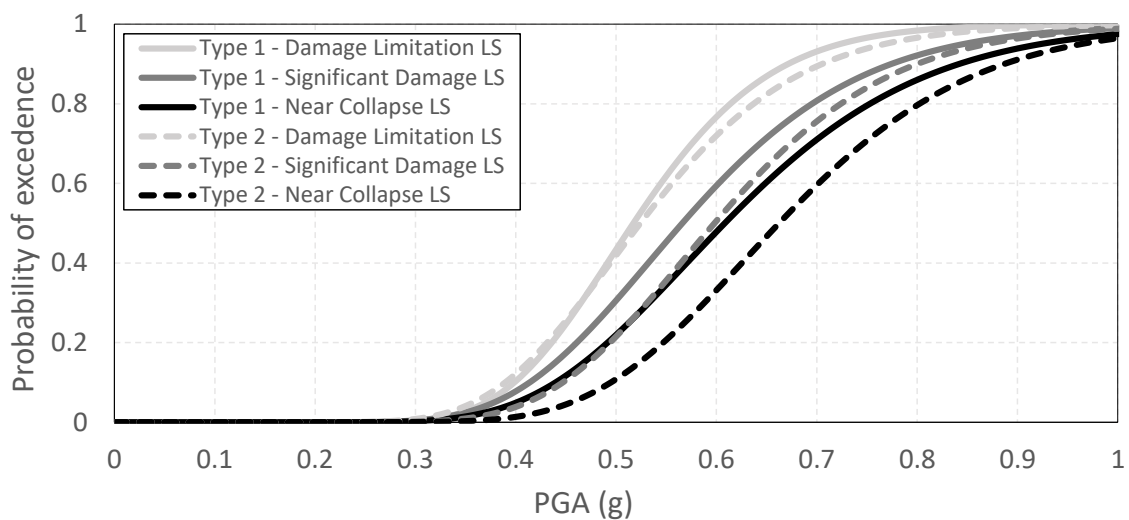
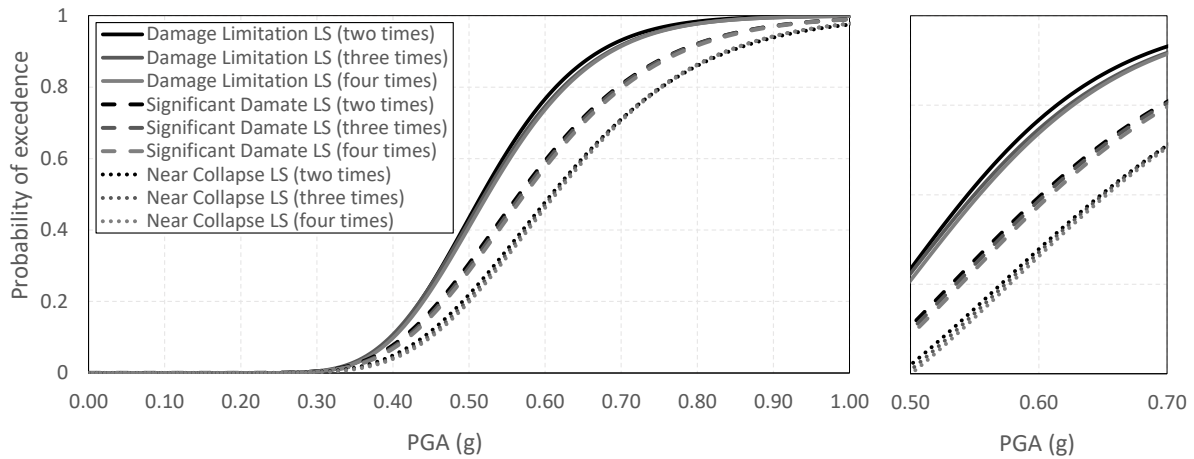
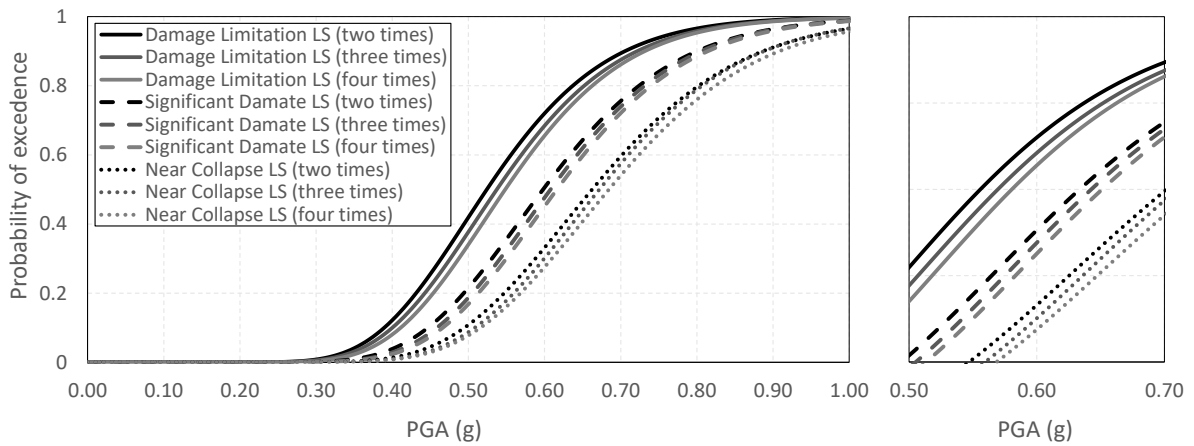


Figure 11. Analytical fragility curves derived due to the application of uniaxial artificial accelerograms.

683 A sensitivity analysis was conducted regarding the role that plays the
684 times that the dynamic response surpasses the CD on the total number of
685 exceeding events. As illustrated in Figure 12a, it can be stated that, when
686 considered Type 1 seismic inputs, the analytical fragility curves do not present
687 significant changes if three or four events are considered. On the contrary, the
688 number of times that the dynamic response is outside the displacement capacity
689 plays a slight influence when applying artificial accelerograms based on a Type 2
690 earthquakes (see Figure 12b). In the case of an IM equal to 0.60 g, the probability
691 of exceeding a Damage Limitation LS presented a reduction of 6.4% when
692 considering that the dynamic response is out of the CD at least four times. A
693 similar behavior was noticed in the case of the remaining two LSs: reductions of
694 5.5% and 5.7% for a Significant Damage and Near Collapse LSs, respectively. It is
695 worth noting that these may be considered as small reduction. Nevertheless,
696 further investigations regarding the optimum number of times that the dynamic
697 response should be outside the displacement capacity need to be conducted. In
698 addition, different criteria can also be used for considering the overcapacity of the
699 structure when subjected to dynamic loadings. The stabilizing effect of the inertial
700 force distributions could be considered by accounting for a dynamic amplification
701 factor of the static dominium. This additional alternative approach also requires
702 further experimental data and will be the subject of future investigations.



(a)



(b)

Figure 12. Sensitivity analysis regarding the number of times that dynamic response was outside the displacement capacity: (a) Type 1 and (b) Type 2 seismic inputs.

703 Following the same approach, the seismic vulnerability of the brick
 704 masonry structure was also assessed considering the influence of additional
 705 components of acceleration (horizontal and vertical). Another set of 2000 analyses
 706 was applied to the numerical model equally distributed between far- and near-
 707 field seismic inputs with a range of PGA between 0.45 g and 0.8 g. For this
 708 assessment, it was also required to define 125 three-component artificial
 709 accelerograms together with 125 uncertain parameters related to the mechanical
 710 properties. The time history analyses were conducted using the automatic routine
 711 considering the new variability of artificial accelerogram. This evaluation was also
 712 focused on the out-of-plane response of the main gable wall, assuming a proper
 713 connection with the return walls. Therefore, the response of the return walls was

714 neglected when assessing the seismic vulnerability of the brick masonry structure.
715 Again, the dynamic response in terms of history of horizontal displacements at the
716 top of the gable wall has been evaluated by means of the CD in order to determine
717 the number of exceeding events for each of the LSs.

718 Figure 13 reports the displacement histories of the three control nodes
719 together with the CD of the different LSs due to the application of three-
720 component artificial accelerograms. It can be evidenced that this multi-directional
721 approach is a powerful tool since it allows the evaluation of the different control
722 nodes with respect to the different LSs. It can be noted that the response of this
723 typology of structure does not only experience displacement in the Y direction
724 (main gable wall), but also in the X direction (return walls) due to the additional
725 component of acceleration. This response is mainly associated with the
726 geometrical characteristics of this structure (U-shape configuration) that implies
727 that the two unconstrained return walls experience an important out-of-plane
728 response. Nonetheless, in this study, the seismic vulnerability assessment was
729 conducted considering only the dynamic response associated with the gable wall
730 and its out-of-plane response, coherently with the experimental campaign. This
731 assumption was also based on the fact that in actual buildings, the return walls
732 are restrained by additional structural elements which limit the out-of-plane
733 response at the corners. After the evaluation of the dynamic response associated
734 with a single control node, it was possible to determine the number of exceeding
735 events which are summarized in Table 5.

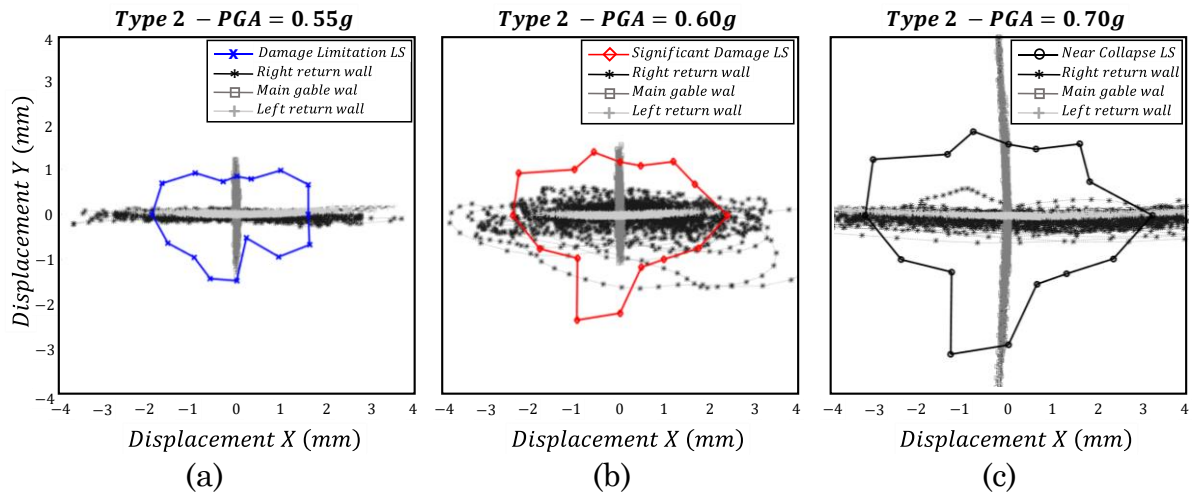


Figure 13. Assessment of seismic performance based on a Capacity Dominium due to the application of three-component artificial accelerograms: (a) Damage Limitation , (b) Significant Damage, and (c) Near Collapse LSs.

736

Table 5. Exceeding events for the derivation of analytical fragility curves due to the application of three-component artificial accelerograms (out of a set of 125).

IM	Number of events	Number of exceeding events					
		Damage Limitation LS		Significant Damage LS		Near Collapse LS	
		Type 1	Type 2	Type 1	Type 2	Type 1	Type 2
0.45 g	125	79	72	57	38	43	21
0.50 g	125	104	99	85	70	67	43
0.55 g	125	113	108	104	92	89	74
0.60 g	125	121	117	116	108	107	97
0.65 g	125	124	125	123	118	119	111
0.70 g	125	125	125	124	124	122	120
0.75 g	125	125	125	125	124	124	122
0.80 g	125	125	125	125	125	125	124

737 The fragility curves derived from the application of far- and near-field
738 three-component seismic inputs are depicted in Figure 14. In the case of far-field
739 seismic input (see solid lines in Figure 14), the occurrence of an event with an
740 intensity of 0.50 g leads to probabilities of exceedance of 82%, 68% and 58% for the
741 Damage Limitation, Significant Damage and Near Collapse LSs, respectively. It
742 can also be noted that the fragility curves are relatively close, especially when
743 considering the last two LSs. This behavior was also evidenced when assessing the
744 seismic vulnerability of the structure subjected to uniaxial inputs. The results
745 associated with the application of near-field seismic inputs are depicted in Figure
746 14 (dashed lines). In this case, the probabilities of exceeding the three LSs
747 correspond to 77%, 54% and 36% for an intensity of 0.50 g. As for the uniaxial
748 input, there is a reduction of probability when comparing the probabilities

749 associated with near- and far-field seismic inputs. The Damage Limitation and
 750 Near Collapse LSs presented the lowest and highest reductions of approximately
 751 5% and 22%, respectively. Another comparison can be conducted considering the
 752 probability of exceedance of the different LSs when applying uniaxial and three-
 753 component artificial accelerograms. The probability of exceedance increased
 754 between 1.9 and 2.7 times for a far-field seismic input with an intensity of 0.50 g.
 755 In the case of near-field seismic input, the application of three-component artificial
 756 accelerograms with a PGA of 0.50 g led to an amplification of the probabilities
 757 ranging between 1.84 and 3.35 times the ones obtained with uniaxial
 758 accelerograms.

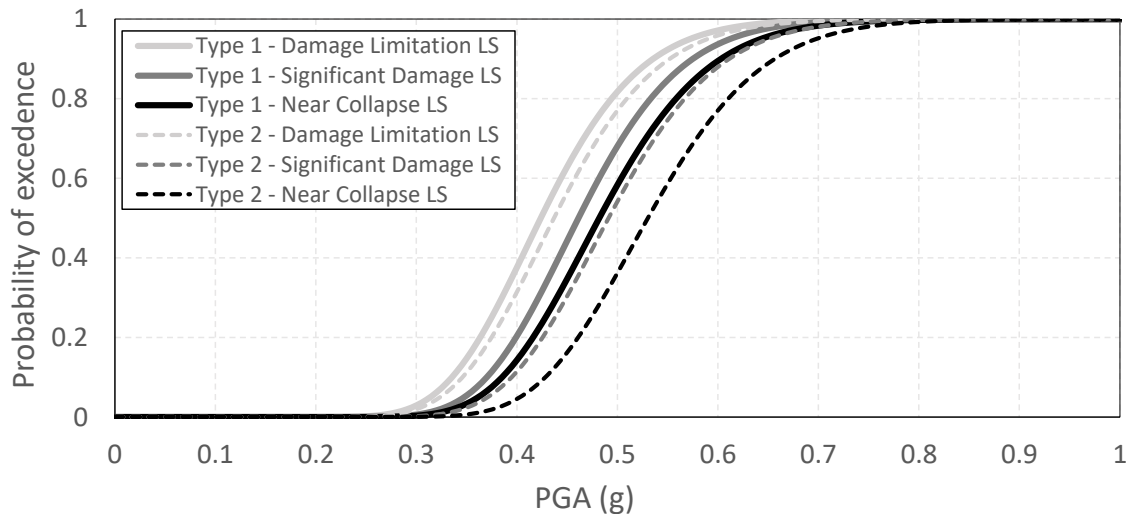


Figure 14. Analytical fragility curves derived due to the application of three-component artificial accelerograms.

759 5. Comparison between fragility curves

760 The last part of this investigation provides a comparison between fragility
 761 curves obtained by means of the proposed analytical approach and an expert-based
 762 formulation. For this purpose, the expert-based fragility functions provided by
 763 Hazus [23], for the building typology denoted as URML, is considered. URML
 764 typology corresponds to URM buildings composed by low-height bearing walls
 765 with one or two stories which somehow resemble to the case study of this
 766 investigation. The comparison between analytical and expert-based fragility
 767 functions also required the definition of three equivalent LSs. The first LS,

768 denoted as Slight Damage, is related to diagonal and stair-step cracking on
769 masonry walls and around openings. The second one, denoted as Moderate
770 Damage, involves the occurrence of diagonal cracking in almost all masonry wall
771 and visible separation from diaphragms. The third LS, denoted as Extensive
772 Damage, consists of extensive damage in most masonry walls and overturning of
773 parapets and gable wall ends. Hazus [23] also provides a set of seismic design
774 levels for the vulnerability assessment of different building typologies, as a
775 function of the date of design and seismic hazard. The Low-code seismic design
776 level was chosen for this comparison (early design codes and moderate seismicity).

777 This comparison involved the definition of single analytical fragility curves
778 for the LSs selected for far- and near-field seismic inputs. For this purpose, an
779 additional round of fitting procedures was conducted considering the total number
780 of exceeding events as the summation of the ones obtained with uniaxial and
781 triaxial accelerograms. The characteristics of the new analytical fragility curves,
782 together with the expert-based ones, are reported in Table 6. Significant
783 differences were clearly identified when comparing the characteristics of the
784 fragility functions based on these two different formulations. The analytical mean
785 values are significantly higher than the ones provided by expert-based formulation
786 regardless of the corresponding equivalent LS. These differences can also be
787 clearly noticed in Figure 15 which shows the fragility curves provided by Hazus
788 [23] together with envelopes of far- and near-field analytical fragility curves. This
789 figure shows that URML structures reach the different LSs when subjected to a
790 lower intensity of seismic input when compared to the analytical envelopes. It can
791 be observed that the occurrence of a seismic event with an intensity of 0.50 g leads
792 to high probabilities of exceedance. In the case of the Slight Damage LS, this
793 probability corresponds to 98%, whereas for the Moderate and Extensive Damage
794 LSs, these values are 92% and 76%, respectively. This comparison demonstrates
795 how the blind use of generic approaches to defining seismic loss of URM structures
796 can provide unrealistic estimates. In addition, it also stresses the necessity of
797 conducting further and more detailed investigations regarding this topic.

Table 6. Mean value and standard deviation associated with analytical and expert-based fragility curves.

EC8-Part3 Limit states	Far -field earthquake		Near-field earthquake		Hazus [23] Limit state	Equivalent PGA Low-code seismic design level	
	θ	B	θ	B		θ	β
Damage Limitation	0.46	0.23	0.47	0.24	Slight Damage	0.14	0.64
Significant Damage	0.50	0.25	0.53	0.23	Moderate Damage	0.20	0.64
Near Collapse	0.53	0.26	0.58	0.23	Extensive Damage	0.32	0.64

798

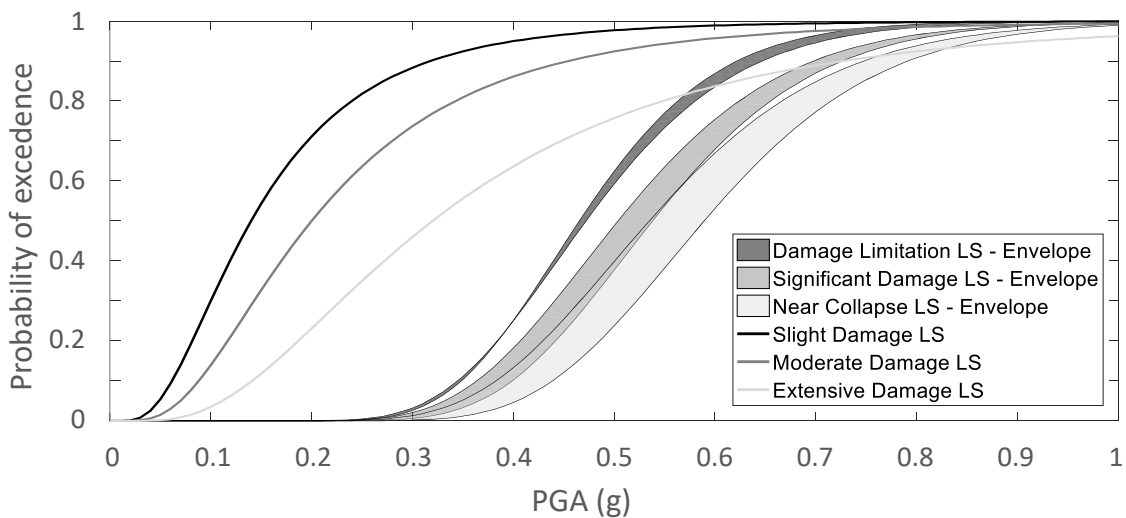


Figure 15. Comparison between analytical and expert-based fragility curves.

799 **6. Final considerations**

800 This paper presented a methodology for assessing the seismic
801 vulnerability of masonry structures characterized by predominant out-of-plane
802 failure mechanisms by means of analytical fragility curves. Such methodology
803 involves the use of an efficient DMEM approach capable of simulating in-plane
804 and out-of-plane mechanisms with a low computational demand. In addition, the
805 proposed methodology is constituted by a series of thorough procedures associated
806 with the definition of seismic input, the definition of limit states and displacement
807 capacities, and the derivation and fitting of analytical fragility curves. Due to the
808 advantages of the adopted modelling approach, the seismic vulnerability
809 assessment involved the application of time history analyses, and it required the
810 definition of suitable seismic input. In addition, the limit states have been defined

811 following specifications provided by standards. Nevertheless, the definition of
812 their corresponding displacement capacity was conducted by means of an
813 alternative procedure, denoted as *Capacity Dominium*, based on multi-directional
814 pushover analyses aiming at a global assessment of structural response. Finally,
815 the derived fragility curves were subjected to a fitting process considering a
816 maximum likelihood approach.

817 In the present study, this methodology has been validated by an initial
818 application to a brick masonry structure which was experimentally and
819 numerically investigated. The generation of the seismic input was conducted
820 based on Type 1 and Type 2 elastic response spectra. Three LSs, namely Damage
821 Limitation, Significant Damage and Near Collapse, were taken into consideration
822 whose capacities were expressed in terms of horizontal top displacements of the
823 main gable wall. These displacements were defined by means of a CD obtained by
824 applying pushover analyses with an incremental angular step of 22.5°.

825 The seismic vulnerability assessment of the brick masonry structure
826 involved two main sources of uncertainty. Such uncertainty was focused on the
827 seismic input as well as the mechanical properties and geometrical properties of
828 the structure. The artificial accelerograms were subjected to eight scaling factors
829 between 0.45 and 0.80, with an incremental step of 0.05. A maximum likelihood
830 procedure was considered for the fitting of the analytical fragility curves allowing
831 the estimation of the probability of exceedance in accordance with the different
832 LSs. This approach required the definition of the actual number of exceeding
833 events which was determined by the use of the CD. Analytical fragility curves
834 associated with the application of far and near-field seismic inputs were derived
835 using the DME model of the brick masonry structure. These results demonstrated
836 the capability of the proposed modeling approach for performing sophisticated
837 analyses for practical applications.

838 In particular, for the analyzed structure, an important difference was
839 found between uniaxial and triaxial seismic input: on average, considering all
840 Limit States and a probability of exceedance of 50%, a 19% reduction of the PGA
841 input is found when comparing the triaxial and the uniaxial seismic inputs.
842 Additionally, the comparison between analytical and expert-based formulations

843 showed some marked differences in terms of fragility curves and their
844 corresponding probabilities of exceedance. Therefore, it is necessary to carefully
845 apply expert-based formulations for a specific location and structural typology,
846 and further investigations associated with the seismic vulnerability of URM
847 structures are required. The definition of a more rigorous procedure for the
848 estimation of the displacement capacity, suitable in a dynamic context and that
849 involves in-plane and out-of-plane mechanisms, constitutes an important task
850 that needs to be investigated in future.

851 In general, it is important to notice that the main steps in this
852 methodology, namely, application of multidirectional pushover analyses for the
853 definition of the displacement capacity as well as nonlinear dynamic analyses for
854 the derivation of fragility curves, require a reasonable computational burden. The
855 analysis demand required for this type of assessment may constitute an important
856 limitation of this methodology; however, it is significantly low when compared to
857 sophisticated and refined FE numerical models characterized by a large number
858 of DOFs. As previously stated, the application of a single nonlinear dynamic
859 analysis was characterized by an average duration of 30 minutes. For this reason,
860 the authors believe that the proposed methodology may allow a thorough
861 assessment of the seismic vulnerability of URM structures.

862 **7. Acknowledgment**

863 The first author gratefully acknowledges the financial support of the
864 Peruvian Institution Innovate Perú/FINCYT (Fondo para la Innovación, Ciencia y
865 Tecnología) through the PhD grant BECA-1-P-078-13. The first author also
866 acknowledges the support and helpful advices provided by Dr. Helder Sousa from
867 the University of Minho, Portugal. The second, third, and fourth authors gratefully
868 acknowledge the financial support of the National Research Project “Advanced
869 mechanical modelling of new materials and structures for the solution of 2020
870 Horizon challenges” (2017–2020), supported by MIUR, Grant No. 2015JW9NJT,
871 Scientific coordinator, Prof. M. Di Paola, prot. n. 2015JW9NJT_017.

8. References

- 873 [1] P. G. Asteris, A. Moropoulou, A. D. Skentou, M. Apostolopoulou, A. Mohebkhah, L.
874 Cavaleri, H. Rodrigues, and H. Varum, "Stochastic Vulnerability Assessment of
875 Masonry Structures: Concepts, Modeling and Restoration Aspects," *Applied*
876 *Sciences*, vol. 9, p. 243, (2019).
- 877 [2] B. R. Ellingwood, "Earthquake risk assessment of building structures," *Reliability*
878 *Engineering & System Safety*, vol. 74, pp. 251-62, (2001).
- 879 [3] T. Rossetto and A. Elnashai, "Derivation of vulnerability functions for European-
880 type RC structures based on observational data," *Engineering Structures*, vol. 25,
881 pp. 1241-63, (2003). doi: 10.1016/S0141-0296(03)00060-9
- 882 [4] *ATC-13, Earthquake damage evaluation data for California*, Applied technology
883 council FEMA contract no. EMW-C-0912, 1985.
- 884 [5] M. Rota, A. Penna, and C. L. Strobbia, "Processing Italian damage data to derive
885 typological fragility curves," *Soil Dynamics and Earthquake Engineering*, vol. 28,
886 pp. 933–947, (2008).
- 887 [6] M. Rota, "Advances in the derivation of fragility curves for masonry buildings,"
888 PhD thesis, European School for Advanced Studies in Reduction of Seismic Risk
889 (ROSE School), Pavia, Italy, (2007).
- 890 [7] *ATC, FEMA-273: NEHRP Guidelines for the seismic rehabilitation of buildings.*
891 *Basic procedures manual*, Applied Technology Council (ATC), 1997.
- 892 [8] *ATC, FEMA-306: Evaluation of earthquake damaged concrete and masonry wall*
893 *buildings. Basic Procedures Manual*, Applied Technology Council (ATC), 1998.
- 894 [9] *Eurocode 8: Design of structures for earthquake resistance – Part 3: General rules,*
895 *seismic actions and rules for buildings, Design Code EN 1998-3*, 2005.
- 896 [10] *NZSEE: Assessment and improvement of the structural performance of buildings*
897 *in earthquakes. New Zealand Society of Earthquake Engineering.*, University of
898 Auckland, 2006.
- 899 [11] *NTC 2008, Decreto Ministeriale 14/1/2008: Norme tecniche per le costruzioni.*,
900 Ministry of Infrastructures and Transportations, 2008.
- 901 [12] G. M. Calvi, "A displacement-based approach for vulnerability evaluation of
902 classes of buildings," *Journal of Earthquake Engineering*, vol. 3, pp. 411-38, (1999).
- 903 [13] A. J. Kappos, G. Panagopoulos, C. Panagiotopoulos, and G. Penelis, "A hybrid
904 method for the vulnerability assessment of R/C and URM buildings.," *Bulletin of*
905 *Earthquake Engineering*, vol. 4, pp. 421-44, (2006).
- 906 [14] P. G. Asteris, "On the structural analysis and seismic protection of historical
907 masonry structures," *The Open Construction and Building Technology Journal*,
908 vol. 2, pp. 124-33, (2008).
- 909 [15] A. Mouyiannou, M. Rota, A. Penna, and G. Magenes, "Identification of suitable
910 limit states for nonlinear dynamic analyses of masonry structures," *Journal of*
911 *Earthquake Engineering*, vol. 18, pp. 231-63, (2014).
- 912 [16] S. Petry and K. Beyer, "Influence of boundary conditions and size effect on the drift
913 capacity of URM walls," *Engineering Structures*, vol. 65, pp. 76-88, (2014).
- 914 [17] S. Lagomarsino and S. Cattari, "Seismic performance of historical masonry
915 structures through pushover and nonlinear dynamic analyses," in *Perspectives on*
916 *European Earthquake Engineering and Seismology*, Springer, (2015), pp. 265-292.
- 917 [18] S. Lagomarsino and S. Cattari, "PERPETUATE guidelines for seismic
918 performance-based assessment of cultural heritage masonry structures," *Bulletin*
919 *of Earthquake Engineering*, vol. 13, pp. 13-47, (2015). doi: 10.1007/s10518-014-
920 9674-1

- 921 [19] M. Rota, A. Penna, and G. Magenes, "A methodology for deriving analytical
922 fragility curves for masonry buildings based on stochastic nonlinear analyses,"
923 *Engineering Structures*, vol. 32, pp. 1312-23, (2010).
- 924 [20] G. Grünthal, "European macroseismic scale 1998 (EMS 1998). Council of Europe,
925 Cahiers du Centre Europe´en de Géodynamique et de Sismologie," p. 15.
- 926 [21] B. Omidvar, B. Gatmiri, and S. Derakhshan, "Experimental vulnerability curves
927 for the residential buildings of Iran," *Natural Hazards*, vol. 60, pp. 345–365,
928 (2012). doi: 10.1007/s11069-011-0019-y
- 929 [22] J. Park, P. Towashiraporn, J. I. Craig, and B. J. Goodno, "Seismic fragility analysis
930 of low-rise unreinforced masonry structures," *Engineering Structures*, vol. 2009,
931 pp. 125-37, (2009).
- 932 [23] *HAZUS 99 earthquake loss estimation methodology, technical manual*, N.-N. I. o.
933 B. Science, 1999.
- 934 [24] L. Pasticier, C. Amadio, and M. Fragiaco, "Non-linear seismic analysis and
935 vulnerability evaluation of a masonry building by means of the SAP2000 V.10
936 code," *Earthquake Engineering & Structural Dynamics*, vol. 37, pp. 467–485,
937 (2008).
- 938 [25] CSI (Computers and Structures Inc.), "SAP2000 v10 Integrated Finite Element
939 Analysis and Design of Structures," (2004), Berkeley,
- 940 [26] P. G. Asteris, M. G. Douvika, M. Apostolopoulou, and A. Moropoulou, "Seismic and
941 Restoration Assessment of Monumental Masonry Structures," *Materials*, vol. 10,
942 p. 895, (2017).
- 943 [27] M. Apostolopoulou, E. Aggelakopoulou, L. Siouta, A. Bakolas, M. G. Douvika, P. G.
944 Asteris, and A. Moropoulou, "A methodological approach for the selection of
945 compatible and performable restoration mortars in seismic hazard areas,"
946 *Construction and Building Materials*, vol. 155, pp. 1-14, (2017).
- 947 [28] P. G. Asteris, M. P. Chronopoulos, C. Z. Chrysostomou, H. Varum, V. Plevris, N.
948 Kyriakides, and V. Silva, "Seismic vulnerability assessment of historical masonry
949 structural systems," *Engineering Structures*, vol. 62-63, pp. 118-134, (2014).
- 950 [29] S. Lagomarsino, A. Penna, A. Galasco, and S. Cattari, "TREMURI program: An
951 equivalent frame model for the nonlinear seismic analysis of masonry buildings,"
952 *Engineering Structures*, vol. 56, pp. 1787-1799, (2013).
- 953 [30] M. A. Erberik, "Generation of fragility curves for Turkish masonry buildings
954 considering in-plane failure modes," *Earthquake Engineering & Structural
955 Dynamics*, vol. 37, pp. 387-405, (2008).
- 956 [31] Y. Mengi, H. D. McNiven, and A. D. Tanrıku, "Models for nonlinear earthquake
957 analysis of brick masonry buildings.," University of California at Berkeley(1992).
- 958 [32] D. D'Ayala, "Force and displacement based vulnerability assessment for
959 traditional buildings," *Bulletin of Earthquake Engineering* vol. 3, pp. 235-65,
960 (2005).
- 961 [33] S. Cattari, S. Frumento, S. Lagomarsino, S. Parodi, and S. Resemini, "Multi-level
962 procedure for the seismic vulnerability assessment of masonry buildings: The case
963 of Sanremo (north-western italy)," in *1st European Conference on Earthquake
964 Engineering and Seismology (ECEES)*, Geneva, Switzerland (2006).
- 965 [34] G. Milani and G. Venturini, "Automatic fragility curve evaluation of masonry
966 churches accounting for partial collapses by means of 3D FE homogenized limit
967 analysis," *Computers and Structures*, vol. 89, pp. 1628-1648, (2011).
- 968 [35] I. Calì, M. Marletta, and B. Pantò, "A new discrete element model for the
969 evaluation of the seismic behaviour of unreinforced masonry buildings,"
970 *Engineering Structures*, vol. 40, pp. 237-338, (2012).
- 971 [36] B. Pantò, F. Cannizzaro, I. Calì, and P. B. Lourenço, "Numerical and
972 experimental validation of a 3D macro-model for the in-plane and out-of-plane

- 973 behaviour of unreinforced masonry walls," *International Journal of Architectural*
974 *Heritage*, (2017). doi: 10.1080/15583058.2017.1325539
- 975 [37] T. Takeda, M. A. Sozen, and N. N. Nielsen, "Reinforced concrete response to
976 simulated earthquakes," *Journal of the Structural Division*, vol. 96, pp. 2557-2573,
977 (1970).
- 978 [38] V. Turnsek and F. Cacovic, "Some experimental result on the strength of brick
979 masonry walls," in *2nd International Brick Masonry Conference*, Stoke-on-Trent,
980 UK (1971).
- 981 [39] C. Chácará, F. Cannizzaro, B. Pantò, I. Caliò, and P. B. Lourenço, "Assessment of
982 the Dynamic Response of Unreinforced Masonry Structures using a Macro-
983 Element Modelling Approach," *Earthquake Engineering and Structural Dynamics*,
984 vol. 47, pp. 2426-46, (2018).
- 985 [40] HISTRA s.r.l, "HiStrA (Historical Structure Analysis) Release 17.2.3," ed. Catania,
986 Italy, (2015).
- 987 [41] F. Cannizzaro, B. Pantò, M. Lepidi, S. Caddemi, and I. Caliò, "Multi-directional
988 seismic assessment of historical masonry buildings by means of macro-element
989 model-ling: Application to a building damaged during the L'Aquila earthquake
990 (Italy)," *Buildings*, vol. 7, (2017).
- 991 [42] J. W. Baker, "Efficient Analytical Fragility Function Fitting Using Dynamic
992 Structural Analysis," *Earthquake Spectra*, vol. 31, pp. 579-99, (2015).
- 993 [43] P. X. Candeias, A. Campos Costa, N. Mendes, A. A. Costa, and P. B. Lourenço,
994 "Experimental Assessment of the Out-of-Plane Performance of Masonry Buildings
995 Through Shaking Table Tests," *International Journal of Architectural Heritage*,
996 vol. 11, pp. 31-58, (2017).
- 997 [44] TNO, "DIANA - DIplacement method ANalyser," (2018), Delft, Netherlands,
- 998 [45] *Eurocode 8: Design of structures for earthquake resistance – Part 1: General rules,*
999 *seismic actions and rules for buildings, EN 1998-1*, 2004.
- 1000 [46] *NP EN 196-8, Eurocode 8: Design of structures for earthquake resistance Part 1:*
1001 *General rules, seismic actions and rules for buildings -Portuguese Institute for*
1002 *Quality*, 2010.
- 1003 [47] D. A. Gasparini and E. H. Vanmarcke, "SIMQKE, A Program for Artificial Motion
1004 Generation: User's Manual and Documentation," (1976), Department of Civil
1005 Engineering, MIT, USA,
- 1006 [48] L. Mendes, "LNEC-SPA: Signal Processing and Analysis Tools for Civil
1007 Engineers," Lisbon, Portugal Patent, 2008.
- 1008 [49] B. Pantò, F. Cannizzaro, S. Caddemi, I. Caliò, C. Chácará, and P. B. Lourenço,
1009 "Nonlinear Modelling of Curved Masonry Structures after Seismic Retrofit
1010 through FRP Reinforcing," *Buildings*, vol. 7, p. 79, (2017). doi:
1011 10.3390/buildings7030079
- 1012 [50] P. B. Lourenço, "Recent advances in masonry modelling : Micromodelling and
1013 homogenisation," in *Multiscale modeling in solid mechanics: Computational*
1014 *approaches*, U. Galvanetto and M. H. Ferri Aliabadi, London, UK, (2009).
- 1015 [51] *JCSS Probability Model Code Part 3: Resistance Models*, Joint Committee of
1016 Structural Safety, 2011.
- 1017 [52] C. Chácará, P. B. Lourenço, B. Pantò, F. Cannizzaro, and I. Caliò, "Macro-Element
1018 Mass Matrix for the Dynamic Assessment of Unreinforced Masonry Structures,"
1019 in *Congreso de Métodos Numéricos en Ingeniería*, Valencia, Spain (2017).

1020

1021